WILD-TYPE AND MATRIX PROTEIN MUTANT STRAINS OF VESICULAR STOMATITIS VIRUS DIFFERENTIALLY MODULATE PODOSOME DEVELOPMENT IN M1 AND M2 MACROPHAGE POPULATIONS

A Thesis
by
DALTON PATRICK SIZEMORE

Submitted to the School of Graduate Studies
at Appalachian State University
in partial fulfillment of the requirements for the degree of
MASTER OF SCIENCE

August 2021
Department of Biology

WILD-TYPE AND MATRIX PROTEIN MUTANT STRAINS OF VESICULAR STOMATITIS VIRUS DIFFERENTIALLY MODULATE PODOSOME DEVELOPMENT IN M1 AND M2 MACROPHAGE POPULATIONS

A Thesis
by
DALTON PATRICK SIZEMORE
August 2021

APPROVED BY:

Darren F. Seals, Ph.D.
Chairperson, Thesis Committee

Maryam Ahmed, Ph.D.
Member, Thesis Committee

Mark E. Venable, Ph.D.
Member, Thesis Committee

Clare Scott Chialvo, Ph.D.
Member, Thesis Committee

Zack E. Murrell, Ph.D.
Chairperson, Department of Biology

Mike McKenzie, Ph.D.
Dean, Cratis D. Williams School of Graduate Studies

Abstract

WILD-TYPE AND MATRIX PROTEIN MUTANT STRAINS OF VESICULAR STOMATITIS VIRUS DIFFERENTIALLY MODULATE PODOSOME DEVELOPMENT IN M1 AND M2 MACROPHAGE POPULATIONS

Dalton Patrick Sizemore
B.S., Appalachian State University
M.S., Appalachian State University

Chairperson: Darren F. Seals, Ph.D.

Macrophages of the tumor microenvironment form cytoskeletal adhesion structures called podosomes that facilitate the invasive behavior of cancer cells through degradation of extracellular matrix proteins. We are interested in investigating whether macrophage podosomes are a therapeutic target of oncolytic strains of vesicular stomatitis virus (VSV). This was accomplished by testing recombinant wild-type (rwt) and matrix (M) protein mutant (rM51R-M) strains of VSV on podosomes in the model THP-1 monocytic leukemia cell line and in macrophages derived from primary blood mononuclear cells (PBMCs). Macrophages exhibit a range of phenotypes between two polarization extremes: the classically-activated, cancer-fighting M1 macrophage and the alternatively-activated, cancer-promoting M2 macrophage. Here we show that while M2 macrophages form more podosomes than M1 macrophages, they are initially less effective at degrading a gelatin matrix. Both VSV strains were able to reduce podosome multiplicity in M2 macrophages and matrix-degrading podosome activity in M1 macrophages, though subtle differences were observed between the different macrophage model systems, VSV strains, and multiplicities of infection. The effects of VSV on M1 macrophages were surprising in that this macrophage subtype was more resistant to VSV infection and cytopathicity. In an attempt to address the

mechanism behind these results, podosome- and polarization-associated transcript levels were monitored in each model system, in each macrophage subtype, and in response to each viral strain. Changes in transcript levels were observed and the influence of enzymes, scaffolding proteins, and actin accessory proteins on podosome development are discussed. Evidence is also provided for how VSV infection may induce a possible hybrid macrophage phenotype with both M1 and M2 characteristics. These results collectively provide further evidence that oncolytic VSV strains not only effectively kill tumor cells but have the potential to act as potent immunogenic agents through the modulation of macrophage populations in the tumor microenvironment.

Acknowledgments

I'd first like to acknowledge my co-advisors for this project, Dr. Darren Seals and Dr. Maryam Ahmed. From the time I first met Dr. Seals and Dr. Ahmed, they were warm and inviting into their labs. I was welcomed and teamed with lab partners who, along with our advisors, nurtured our growth and maturity as scientists and as people. In addition, Dr. George Whitesides, Dr. Keith Barlow, Dr. Jamison McCann, and Dr. Kiani Gardner, all of whom were instructors at Guilford Technical Community College during my time there and encouraged me to continue my pursuit into biological education and research.

I'd also like to thank the many professors in our department, specifically all of those who had some role in my education while at Appalachian State including Dr. Mark Venable and Dr. Clare Scott Chialvo, who have worked to read materials, watch my presentations, and serve as members of my thesis committee. Also, to Dr. Zack Murrell, our department chair, who supported me getting involved in a research project as my undergraduate advisor and supported me in staying on to obtain my Master's and Dr. Ray Williams who has helped me work through the issues that have come up along the way as a student and student leader at Appalachian State. I'd like to especially recognize Dr. Guichian Hou for providing microscopy training as well as the College of Arts and Sciences for the creation and continual funding of the Dewel Microscopy Center at Appalachian State University.

Most of all, I'd like to thank each and every member of our lab and our department who have supported me with lab maintenance, experimentation, conversations about research, and general friendship. I'd like to specify several individuals for their assistance: Megan Polzin for laying the foundations of this project and your willingness to always get Mexican food with me; Brewer Logan for supporting my initial training, continual

conversations about our research, and assisting me in getting post-graduation plans off the ground; Dylan Fehl and Dakota Goad for their assistance in training and development of protocols of which I was unfamiliar; Austin Simmons for countless hours of conversations, sharpening my skills to explain our research, and his friendship during hard times of the pandemic, as well as his assistance in keeping our projects going during this time; and to Taylor Strope who sat with me during long hours of experimentation, talked with me about what was going on within my study, and continuing those conversations long after she moved halfway across the country to attend her PhD program. There are many, many others have assisted me along the way, including those who I assisted in training: Carmen Montero, Audrey Patterson, Melissa Rowe, Gabrianne Ivey and Emma Wandscher, and those who supported me as acquaintances: Emily Lucero, Jamison Slate, Sylas Owen, and so, so many others outside of the Seals and Ahmed labs.

Dedication

While my dedication for this thesis could be hundreds of pages long if I took the time to thank each and every person who has motivated me to pursue the best in myself, I want to dedicate this work to my grandfather, Charlie Sizemore. He stepped into the role of my father figure when my father left my life and showed myself and our family what it was to work hard and to take care of your family. Without his influence during my childhood and into my adulthood, the strength and personality he helped instill in me, and the work ethic he and my grandmother, Mary Lou, instilled in my mom and myself, this would not be possible. Although he is no longer with us, I do believe he would be proud in me and what I have accomplished.

I also want to dedicate this to anyone whose parents have left them and their family by choice. Although life during all stages is extremely difficult and you'll see friends and others who have the support, nurture, and love by all of their family members, don't let it be a personal reflection on you. Sometime down the road, which may take many years like it did for me, you'll see why it happened and how you have become a better person because they've left your life. Upon reflection upon my own life, I know I wouldn't be the person I am today or have come close to completing a research project of this nature and magnitude if my "sperm donor" would have stayed in mine.

Table of Contents

Foreword

Parts of this thesis will be submitted to *Journal of Virology*, an international peer-reviewed journal owned and published by the American Society for Microbiology; this thesis has been formatted according to the style guide for that journal.

CHAPTER 1: INTRODUCTION

M1 and M2 Macrophage Classification

Macrophages are tissue resident cells of the innate immune system that defend against pathogenic infection and repair injured tissue (1). They are derived from blood circulating monocytes. In response to infection or injury, these monocytes traverse the blood vessel wall by extravasation where they subsequently differentiate into macrophages and polarize to either classically-activated M1 or alternatively-activated M2 macrophages. M1 polarization is induced by bacterial cell wall components; *i.e.* lipopolysaccharides (LPS) and cytokines like interferon gamma (IFN-γ) or tumor necrosis factor alpha (TNF-α) (2). M1 macrophages are characterized by the expression of phosphorylated signal transducer and activator of transcription 1 (p-STAT1), major histocompatibility complex class II (MHC-II), and the co-stimulatory molecules CD80/86, in addition to the secretion of the pro-inflammatory cytokines interleukin-6 (IL-6), IL-1β, and TNF-α, as well as reactive nitrogen species. Their main function is to phagocytose pathogens as part of the innate immune response and to present antigens for the adaptive immune response to infection (3-5). M2 macrophages are polarized by complement proteins, apoptotic cellular debris, IL-4, IL-13, IL-10, and transforming growth factor beta (TGF-β), which are released at sites of tissue damage (2). M2 macrophages are characterized by the surface marker CD204, and the secretion of vascular endothelial growth factor (VEGF), IL-10, and matrix metalloproteinase 9 (MMP-9), and whose main function is to assist in anti-inflammatory responses, extracellular matrix (ECM) remodeling, and wound healing. More extensive research has shown that macrophages actually fall along a spectrum of phenotypes between these M1 and M2

extremes (6). Moreover, these are highly plastic cells that have the ability to switch phenotypes in response to changing environmental conditions.

Tumor-associated Macrophages Help or Hinder Tumor Growth

Macrophages are the predominant immune cell type within the tumor microenvironment (TME) where they are commonly referred to as tumor-associated macrophages (TAMs) (6). TAMs also fall along the phenotypic spectrum from M1 to M2 and can thereby help or hinder tumor growth and disease progression. M1-like TAMs secrete reactive oxygen and nitrogen species, phagocytose tumor cell debris, recruit additional immune cells, and present the tumor antigens to T-cells to enable the adaptive anti-tumor immune response. In contrast, M2-like TAMs are predictive of poor patient prognosis. M2 macrophages release cytokines (IL-10, IL-4, IL-13) that counteract the pro-inflammatory immune response within the TME leading to suppression of anti-tumor immunity. They also express growth factors such as VEGF, fibroblast growth factor (FGF), insulin-like growth factor 1 (IFG-1), C-C motif chemokine ligand 2 (CCL2), and placental growth factor (PGF) that discourage apoptosis, promote cancer cell proliferation, and stimulate the development of blood vessels throughout tumor tissues as part of angiogenesis, all of which are hallmarks of cancer progression (2, 7). Development of blood vessels can also lead to promotion of another hallmark of cancer, metastasis, whereby the tumor cells spread to distant sites in the body. M2 macrophages also assist directly in metastasis through their ability to reach into and degrade the ECM that surrounds tumor tissue (8-14). This matrix-degradative function of macrophages can be directly correlated to the number and activity of cytoskeletal structures called podosomes.

Macrophage Podosome Structure

Podosomes are dynamic, actin-based, cell surface protrusions that naturally occur in invasive cell types, including cells of the myeloid lineage (15). These cytoskeletal structures generate force from within their filamentous actin (F-actin) core that, in conjunction with actin accessory proteins, push into the ECM where integrin receptors can support ECM adhesion and where membrane-associated and secreted MMPs degrade the ECM to support mobility throughout tissues (16-18).

F-Actin Cores of Podosomes

The primary component of the podosome core is F-actin (15). This core is synthesized from monomers composed of globular actin (G-actin) bound to ATP that polymerize with the aid of actin nucleation proteins. F-actin is easily identified via microscopy using fluorescently-conjugated phalloidin as a stain, with the core structure having a punctate dot-like appearance with a diameter between 0.5 and 1.0 μm (15, 19).

The F-actin core is surrounded by actin assembly proteins including the actin-related protein 2/3 complex (Arp 2/3), cortactin, Wiskott-Aldrich Syndrome protein (WASp), WASp-interacting protein (WIP), dynamin 2, and gelsolin (19, 20). These proteins act together to regulate actin polymerization and stabilization within the core. The core provides the structural stability needed to maintain the podosome as it probes its environment to allow for adhesion to and movement into the tissue.

Outer Rings of Podosomes

The outer ring of the podosome consists of adhesion proteins that anchor the F-actin

core to the lipid membrane (20-23). This adhesive ring complex consists of α-actinin bound to the core of the podosome surrounded by an array of radial actin fibers (20, 24). This ring also contains adhesion proteins comprised of vinculin, paxillin, talin, protein tyrosine kinase 2 beta (Pyk2), and gelsolin, all of which bind actin microfilaments to cell surface integrin receptors membrane (25-28). The entirety of this complex of proteins stabilizes the core of the podosome to the membrane and to transmembrane integrin receptors.

Cap Structure of Podosomes

The cap structure sitting atop the F-actin core at the base of the podosome where it begins to push out from the cell serves an important role in mechanosensing and is an area of extensive regulation, including stabilization of the podosome core via prevention of actin depolymerization (21, 22, 29-33). The ability of the podosome to "sense" their surrounding environment, including the rigidity of the ECM through the cap, allows for actin assembly proteins to adapt with increased stiffness in the core of the podosome. This is accomplished by synthesizing new actin microfilaments or by bundling the existing actin microfilaments together. In addition to the increased stiffness in the podosome core, the cap serves as the docking point for secretory vesicles containing the MMPs that facilitate ECM degradation, thus allowing the podosome to extend into the tissue to greater lengths.

Stages of Macrophage Podosome Development

The synthesis of podosomes can be divided into four distinct stages: initiation, assembly, maturation, and turnover. Based on timing, macrophage podosomes are sorted into one of two distinct populations, precursors or successors. Precursors are defined by their

larger structure, shorter lifetime, and their presence at the leading edge of migrating cells (1, 33). Successors are characterized by having a smaller structure, longer lifetime/increased stability, and localizing in the middle of the cell, or right behind the precursors in migrating cells.

Macrophage Podosome Initiation

The key signal for macrophage podosome initiation is attachment of the cell to a substrate, since podosomes are only observed in adherent cells (15). Attachment of cells leads to clustering and activation of integrins and signaling by class III receptor tyrosine kinases, including Feline McDonough Sarcoma (FMS) family and recepteur d'originie nantais (RON) family receptors (34, 35). Protein kinase C (PKC) activity is also an important upstream signal for podosome formation, as podosome initiation can be induced by PKC-activating agents, such as the phorbol ester 12-myristate 13-acetate PMA or the protein macrophage colony stimulating factor 1 (M-CSF, CSF-1) (36-38). It also leads to activation of non-receptor tyrosine kinases like the Src family kinase member Hck and focal adhesion kinase (FAK) (39, 40). FAK is involved in coordinated changes in actin structures by phosphorylation of GTPase activating proteins and guanine nucleotide-exchange factors that modulate Rho-type GTPases, leading to recruitment of WASp and of subunits of the Arp2/3 complex (41, 42).

Macrophage Podosome Assembly

As podosome initiation is occurring, assembly of the podosome structure commences as well (19). Actin assembly proteins, mediated by the Arp 2/3 complex, are recruited to the

area of podosome initiation by the lipids phosphatidylinositol 3,4-bisphosphate and phosphatidylinositol 3,4,5-trisphosphate where actin polymerization subsequently occurs. Src family kinases then begin to phosphorylate downstream targets, including the podosome scaffolding protein tyrosine kinase substrate 5, or Tks5 (43-49). This scaffolding protein is recruited by phosphatidylinositol 3-phosphate and phosphatidylinositol 3,4-bisphosphate via its lipid-binding phox homology (PX) domain where it then recruits other proteins, including cortactin, an actin polymerization promoter and actin microfilament rearranger, AFAP110, and p130Cas, through one or more of its five Src homology 3 (SH3) domains. Inhibition of Src family kinases has been shown to suppress podosome formation, while constitutive activation of Hck has been shown to increase podosome formation (45, 50).

In addition, because of the prominence of its F-actin core, the availability of ATP-bound G-actin monomers also acts as a podosome regulator. Other actin-associated proteins, including members of the WASp family and Arp 2/3, are requisite for podosome regulation and their absence leads to disruption of podosomes globally (15, 49, 51-55).

Macrophage Podosome Maturation

As the core of podosome machinery is being built, a ring begins to form around it (19). Further development of the podosome ring and the start of ECM degradation are a key indicator of the progression from the assembly phase to the maturation phase of podosome development. Whereas Tks5 recruits cortactin to podosomes, cortactin, in turn, regulates the localization and secretion of MMPs (56). Cortactin recruitment to podosomes immediately precedes the trafficking of protease-containing vesicles. MMPs are trafficked to the podosomes via kinesin motor proteins, which transport cargo along microtubules (17, 57,

58). MMPs are then either presented at the cell surface or are secreted from the cell where they facilitate ECM degradation (15, 17, 59, 60).

Macrophage Podosome Turnover

Podosome lifetime in macrophages ranges from 0.5 to 14 minutes with a median of 2.5 minutes (15, 61). A small percentage of macrophage podosomes extend their lifetimes to over 30 minutes (15, 31). Podosome turnover may occur when cap proteins disassemble and the local concentrations of the formin INF2, an actin nucleation protein, begin to decrease and local concentrations of gelsolin, an actin-severing protein, begin to increase, reducing more actin microfilaments than are synthesized (16, 62). Fascin-mediated actin-bundling at podosome caps is another mechanism of macrophage podosome turnover. The promotion of more bundles of F-actin relative to branches of F-actin leads to shrinkage and turnover of the podosome.

M2 Macrophage Podosomes Facilitate Metastatic Disease

As macrophages are polarized to M1 or M2 phenotypes, the number of podosomes changes significantly (24, 29, 63). M2 macrophages have significantly more podosomes than do their M1 counterparts (64). Moreover, human M2 macrophages derived from peripheral blood monocytes as well as murine M2 macrophages derived from the bone marrow all migrate through fibrillar collagen, representative of loosely connected ECM, and Matrigel, representative of highly connected ECM, at significantly higher rates than do M1 macrophages (35). They also have higher amounts of the more highly organized podosome superstructures called rosettes (29). Murine bone marrow-derived M2 macrophages also

degrade significantly more gelatin (the denatured collagen component of the ECM) than do M1 macrophages. The increased ECM degradation, migration, and invasion seen in M2 macrophages are all directly correlated to the number of podosomes these macrophages have. Tumors with higher M2/M1 macrophage ratios also demonstrate higher rates of invasion and metastasis (9, 11-13, 65-67). Presumably this is due to the ability of M2 macrophage podosomes to degrade and remodel the ECM allowing for tissue invasion by neighboring cancer cells, intravasation of blood vessels, and colonization of distant metastatic sites. The use of podosome-directed therapeutics may thereby reduce overall levels of tumor viability and metastasis.

Podosome-directed Cancer Therapeutics are Lacking

Current cancer therapies mostly focus on cancer cells by either inhibiting growth, arresting the cell cycle, or stimulating apoptosis and tumor shrinkage (68). Currently, there is an increase in the use of therapies that harness the natural cancer-fighting abilities of the immune system (69). This includes the introduction of exogenous immune-stimulating cytokines and monoclonal antibodies, or the removal of immune cells from the patient, "training" those cells *in vitro* to attack the patient's own cancer cells, and then re-insertion back into the patient for a more targeted adaptive immune cell response. However, no current designated therapeutic treatment is used to block the fundamental mechanisms involved in podosome-mediated metastasis. A previous study used QIAGEN Ingenuity Pathway Analysis (IPA) to search for inhibitors of the podosome-related invadopodia found in cancer cell lines (68). The IPA database, which assigns drugs that are FDA-approved or are in pre-clinical stages of drug development to protein pathways, only identified 59 protein targets that

promote migration, invasion, and/or induce invadopodia development. And of the 2500 clinical trials against breast cancer, head and neck cancer, and glioblastoma multiforme, less than 100 demonstrated the successful prevention of metastasis. Two drugs, denosumab (an antibody specific to receptor activator of nuclear factor kappa-B ligand (RANKL)) and trastuzumab (an antibody specific to the epidermal growth factor receptor HER2), were shown to target invadopodia-associated genes. While there are no currently approved therapeutics that directly target macrophage podosomes, a recent study using oncolytic vesicular stomatitis virus (VSV) has shown promise in not only killing cancer cells, but also reducing the overall amount of podosomes within M2 macrophage populations (64, 70-76).

Oncolytic Vesicular Stomatitis Virus

Oncolytic viruses like VSV have the ability to target and kill cancer cells over normal cells, either naturally or after genetic manipulation (70-74, 77-80). Although different oncolytic viruses have specific mechanisms for targeting cancer cells, VSV infects and replicates in cancer cells that have defects in anti-viral pathways, thus rendering them susceptible to virus-induced cytopathicity. This not only releases viral progeny capable of spreading through the TME to kill surrounding cancerous cells, but the lysis of cancer cells also releases tumor antigens that increase local inflammation and induce a systemic immune response that is pre-programmed to be both anti-viral and anti-tumoral. In this study, the ability of VSV to modulate podosome development as another potential therapeutic benefit was investigated.

VSV is a negative stranded RNA virus of the family *Rhabdoviridae* (81). It is an arthropod-borne virus that primarily affects rodents, cattle, swine, and horses via insect

vectors like sandflies, black flies, and mosquitos. In animals, VSV infection produces an acute condition similar to foot and mouth disease, but in humans VSV infection is typically asymptomatic, producing at most flu-like symptoms.

VSV replication is similar to other negative-strand RNA viruses. The viral glycoprotein binds to the surface of the host cell via the low-density lipoprotein receptor (LDLR) and enters the cell through clathrin-dependent endocytosis (81-83). Once the clathrin-coated endosome drops to a pH of 6.2, the viral glycoprotein envelope fuses with the endosomal membrane, thus releasing the nucleoprotein-encapsulated RNA genome into the cytoplasm (84-86). Within the nucleocapsid, the large polymerase and phosphoprotein initiate synthesis of viral mRNAs that are translated by the host cell translation machinery. Viral genome replication occurs entirely in the cytoplasm and as viral proteins are expressed, viral components assemble to form mature viral particles that are released through budding into the cellular environment.

The 11 kilobase genome of VSV only encodes five proteins, and in the following order: nucleoprotein (N), phosphoprotein (P), matrix protein (M), glycoprotein (G), and the large polymerase (L) (81). The matrix (M) protein of VSV was discovered based on its role in virus assembly where it binds the helical nucleoprotein core of the virus to the cytoplasmic surface of the infected cell's plasma membrane during budding (87). Additionally, the M protein disables host cell gene expression by either shutting down the RNA polymerases I, II, and III (except in the case of 5S rRNA with RNA polymerase III) involved in host cell transcription or by binding to the nucleoporin Nup98 and blocking nucleocytoplasmic transport of mRNAs (81, 82, 88). In this way the M protein disrupts a primary viral defense

mechanism in the host cell involving the type I interferon (IFN) pathway and thereby maximizes infection and replication efficiency.

Type I Interferon Anti-viral Defense Pathways

The type I IFN pathway is the main cellular defense pathway against the majority of viruses. The type I IFN family includes 13 semi-homologous interferon alphas (IFN-α), one interferon beta (IFN-β), and six other poorly defined single gene interferon products (89). Both IFN-α and IFN-β act through autocrine and paracrine signaling to induce an anti-viral state in host cells (90, 91). Released type I IFNs bind to type I IFN receptors (IFNARs) on target cells activating the Janus kinase (JAK)-STAT pathway which leads to the transcription of IFN-stimulated genes (ISGs) with anti-viral functions. This pathway thus limits the spread of viruses, modulates the innate immune response in a manner that promotes antigen presentation and natural killer cell functions, and activates the adaptive immune system to promote antigen-specific T and B cell responses and immunological memory.

The type I IFN pathway is induced through the detection of VSV via one of several toll-like receptors (TLR4, TLR7, TLR13) or when cytosolic proteins like retinoic acid-inducible gene I (RIG-1) or melanoma differentiation-associated gene 5 (MDA5) recognize viral mRNA (92-94). Following detection of VSV, diverse downstream pathways converge on a handful of key molecules, such as the IFN-regulatory factor (IRF) family of transcription factors that subsequently activate transcription of the genes encoding IFN-α and IFN-β (90).

Because of the unique abilities of the M protein of VSV to block host gene transcription and nucleocytoplasmic transport, VSV has the ability to thwart this key anti-

viral defense pathway. However, in using VSV as an oncolytic agent, it would be beneficial to express pro-inflammatory cytokines, recruit additional immune cells to the TME, and potentially reprogram M2-like TAMs to an M1 phenotype. This would require a mutant form of the M protein that retains all its capabilities with the exception of blocking host transcription and transport of mRNA.

VSV M Protein Mutants

Several M protein mutant strains of VSV have been investigated as selective anti-cancer agents with the most notable being VSV-M51R-M and VSV-ΔM51 (95, 96). The VSV-M51R strain has a single point mutation in amino acid 51 of the M protein sequence that switches the methionine to an arginine, while VSV-ΔM51 has a deletion of this methionine. The M proteins of both strains are fully functional in their virus assembly functions but have defects in their ability to suppress host gene expression, including expression of genes in the type I IFN anti-viral response. Although devoid of the ability to suppress the type I IFN response, these viruses can still induce apoptosis in cancer cells (97, 98). Because of these characteristics, M protein mutant viruses such as these are currently being developed as safer, more onco-selective viral strains relative to wild-type strains of VSV.

VSV's Impact on Macrophage Podosomes

While VSV is well-appreciated as an oncolytic agent, its impact on macrophages in general, and TAMs in particular, is far less clear. Recent data using recombinant strains of VSV expressing GFP showed that VSV was capable of replicating within the THP-1

monocytic leukemia cell line, and the extent of replication was macrophage subtype-dependent (64). For example, both recombinant wild-type (rwt-GFP) and M protein mutant (rM51R-GFP) strains of VSV were visualized in a high percentage of M2 THP-1 macrophages, but there was no visualization of these viral strains in M1 macrophages. This is consistent with previous studies indicating that M1 polarizing signals induce the anti-viral type I IFN pathway, thus rendering these macrophages resistant to viral infection (99). The permissibility of M2 THP-1 macrophage to viral replication also explains their susceptibility to killing by the virus or their ability to upregulate the type I IFN pathway leading to an inflammatory M1-like phenotype. Indeed, rwt virus does kill ~70% of M2 THP-1 macrophages while r-M51R-M virus induces a significant upregulation of proteins associated with M1 polarization, including p-STAT1, the cell surface marker CD80, and the cytokine TNF-α (64, 100). By taking advantage of their natural plasticity, perhaps rM51R-M virus may be able to convert tumor-promoting M2 TAMs into tumor-fighting M1 TAMs.

In this same study, M2 THP-1 derived macrophages produced significantly more podosomes than M1 macrophages (64). Moreover, M2 macrophage podosome numbers significantly decreased following infection with rwt virus, while M1 macrophage podosome number was unaffected. This study did not propose or address potential mechanisms of how VSV decreased M2 macrophage podosome number. It also did not address the effect of VSV on the ECM degradation function of the podosomes in either macrophage subtype. Finally, this previous work was done in the established THP-1 monocytic leukemia cell line used to model monocyte/macrophage behavior, not in primary monocyte/macrophage populations. Such were the goals of this study: to determine whether VSV's anti-cancer arsenal includes targeting TAM podosome development and activity.

CHAPTER 2: MATERIALS AND METHODS

THP-1 Cell Culture and Macrophage Polarization

The human monocytic leukemia cell line THP-1 was cultured at 37°C and 5% CO_2 in RPMI-1640 (Corning) media supplemented with 0.3 g/L L-glutamine, 10% fetal bovine serum (Atlanta Biologicals), and 0.05 mM β-mercaptoethanol (MP Biomedicals). Cells were grown to a concentration of 8-10 x 10^5 cells/mL, after which they were diluted back to 2 x 10^5 cells/ml using fresh media. To initiate macrophage differentiation, THP-1 monocytes were seeded into cell culture dishes or plates per experimental specifications. The cells were cultured in media containing 25 nM PMA (Sigma-Aldrich) for 24 hours. The cells were then further polarized to different macrophage subtypes by washing with sterile PBS and treating for 48 hours with 20 ng/mL LPS (Sigma-Aldrich), 20 ng/mL IFN-γ (BioLegend), and 25 nM PMA for M1 macrophages or 20 ng/mL IL-4 (BioLegend), 20 ng/mL IL-13 (BioLegend), and 25 nM PMA for M2 macrophages. PMA was prepared as a 1000X stock solution in DMSO. LPS, IFN-γ, IL-4, and IL-13 were prepared as 1000X stock solutions in a 0.05% BSA in PBS solution and stored at -80°C as small aliquots. Stock solutions were frozen and thawed no more than two times.

Peripheral Blood Collection and Primary Monocyte Isolation

A total of 50 mL of whole blood was drawn from healthy, 21-29-year-old volunteers who were non-smoking, not pregnant, had not given birth within the last year, and were not on any medication regiment known to have an effect on the immune system. Blood was drawn from the median cubital vein in the antecubital fossa via 21-gauge butterfly needle

draw set (Becton, Dickinson and Co.) connected to a Vacutainer holder (Becton, Dickinson and Co.) and 10 mL sodium heparin Vacutainer tubes (Becton, Dickinson and Co.). Procedures for human subjects research were approved by Appalachian State University's Institutional Review Board under protocol #20-0071.

Collected peripheral blood (50 mL) was equally distributed between two 50mL conical tubes. To each conical tube, 25 mL of PBS was added before the tube was inverted several times. A measure of 25 mL of the blood/PBS solution was then carefully layered on 18.5 mL of Ficoll-Paque PREMIUM density gradient media (Cytiva Life Sciences) in a fresh, sterile 50 mL conical tube. All conical tubes were then centrifuged at 400xg for 40 minutes at 22°C without assistive breaking. The upper layer containing plasma was removed, leaving the mononuclear layer undisturbed at the interface. The mononuclear cells were collected (~10 mL per tube spun) and transferred to a sterile 15mL conical tube. Here they were washed twice by diluting with 5 mL of PBS, inverting several times, and centrifuging at 400xg for 10 minutes at 22°C. Viable cells were counted on a hemocytometer in a 1:1 mixture with 0.4% trypan blue.

Primary Monocyte Culture and Macrophage Polarization

PBMCs, collected and enumerated via previously described methods, were resuspended in RPMI-1640 (Corning) formulated with 0.3g/L L-glutamine, 10% fetal bovine serum (Atlanta Biologicals), and 0.05 mM 2-mercaptoethanol (MP Biomedicals), and seeded into plates at 37°C and 5% CO_2 per experimental specifications. The cells were then cultured for 24 hours allowing monocytes to adhere to the plate.

After the media containing non-adherent cells was removed, the attached monocytes were washed thrice in 1mL PBS followed immediately by vacuum aspiration. The culture was then replenished with media supplemented with 25 nM M-CSF in 0.5% BSA in PBS (BioLegend) for 48 hours, stimulating the monocytes to differentiate into macrophages. The cells were then further polarized for 48 hours with 20 ng/mL LPS (Sigma-Aldrich) and 20 ng/mL IFN-γ (BioLegend) for M1 macrophages or 20 ng/mL IL-4 (BioLegend) and 20 ng/mL IL-13 (BioLegend) for M2 macrophages.

VSV Strains

Recombinant wild-type (rwt) and recombinant matrix (M) protein mutant (rM51R-M) strains of VSV, as well as the rwt and rM51R-M viruses expressing green fluorescent protein (rwt-GFP and rM51R-GFP) were a generous gift from Dr. Douglas Lyles of the Wake Forest University School of Medicine (Winston-Salem, NC) and have been previously described (101). Virus stocks were prepared in baby hamster kidney (BHK) cells using methods described previously (97). Viruses were applied to THP-1 or primary M1 or M2 macrophage cultures per experimental specifications.

Production of FITC-Conjugated Gelatin Coverslips

Glass coverslips (Carolina Biological) were pre-cleaned in a 12-well plate overlaid with 20% nitric acid in PBS for 30 minutes followed by three washes in PBS. Coverslips were then incubated in 50 μg/mL poly-L-lysine (Electron Microscopy Sciences) in PBS for 20 minutes and washed three times in 1 mL PBS. Coverslips were then incubated in 0.5% glutaraldehyde (Electron Microscopy Sciences) in distilled water for 15 minutes and washed

three times in 1 mL PBS. Unlabeled gelatin was made using 1.25 g porcine skin gelatin (Sigma-Aldrich), 1.25 g sucrose (Sigma-Aldrich), and PBS to a final volume of 50 mL and was warmed to 40°C to completely dissolve the gelatin. Unlabeled gelatin was stored in 10 mL aliquots at 4°C. FITC-conjugated porcine gelatin (Invitrogen) was reconstituted according to the manufacturer's protocol and stored in 500 μL aliquots in amber microfuge tubes at 4°C. Working gelatin solutions were based on a mixture of 8 parts unlabeled gelatin to 1 part labeled gelatin to make enough for 100 μL per coverslip. The mixture was brought to 40°C and was pipetted onto each coverslip. Excess gelatin on the coverslips was immediately removed via micropippetting at the most distant point in the well from the coverslip. The coverslips were then incubated for 15 minutes in the dark at room temperature. Coverslips were the treated with 1 mL sodium borohydride (Sigma-Aldrich) at a concentration of 5 mg/mL in PBS for 12 minutes before being washed three additional times in PBS. Coverslips were then sterilized for 30 minutes in 70% ethanol before being quenched for at least 24 hours in cell culture media at 37°C.

Gelatin Degradation Assay

To examine the ability of macrophage podosomes to degrade gelatin, 1 x 10^7 THP-1 monocytes were first seeded in a 10cm dish and were polarized using previously described methods. Upon completion of the 72-hour polarization period, the media was removed and the cells were washed once in PBS. Cells were then separated from the dish with 5 mL of Accutase (Corning) at 37°C and 5% CO_2 for 30-60 minutes. After counting the cells on a hemocytometer in the presence of trypan blue, 1 x10^5 THP-1 macrophages were seeded into 12-well plates containing a single FITC-conjugated gelatin-coated coverslip in a final volume

of 1 mL. After allowing to adhere for two hours, the macrophages were then infected with or without (mock) rwt or rM51R-M virus at a multiplicity of infection (MOI) of 1 or 10 plaque forming units (pfu)/ml for 6, 12, and 24 hours. Post-infection, each well was aspirated, washed with 1 mL PBS, and the cells fixed in 1 mL 3% formaldehyde (Electron Microscopy Sciences) in PBS for 15 minutes at room temperature. After another PBS wash, the cells were permeabilized in 1 mL 0.4% Triton X-100 (MilliporeSigma) in PBS for 10 minutes at room temperature, followed by another three washes in 1 mL PBS. Coverslips were then mounted onto glass microscope slides using 15μL aliquots of ProLong Gold Antifade Mounting Media with DAPI (Cell Signaling). The coverslips were then cured in the dark overnight, sealed with nail polish, and imaged by fluorescence microscopy.

Gelatin Degradation Imaging and Quantification

Each coverslip was imaged using an Olympus IX81 microscope with an Olympus DP71 camera at 20x magnification using CellSens Dimensions software. Ten, random images were taken for each coverslip. Images were analyzed using ImageJ 1.8.0 software. Scale and measurements were selected by choosing "Analyze > Set measurements." Using the fluorescent gelatin image, the total area of degradation was calculated. The threshold of the image was set (Image > Adjust > Threshold) to the upper and lower intensity values to select the areas of degradation. In some cases, the gelatin was not completely flat when images were acquired. Corrections for uneven background illumination across the gelatin were accomplished by subtracting the background (Process > Subtract background) or by filtering with a bandpass filter (Process > FTT > Bandpass Filter). The total area degraded was measured by particle analysis (Analyze > Analyze Particles). In the Analyzes Particles

Window, a particle size > 10 was chosen to remove noise from the selection. “Display results” and “Summarize” were checked to show measurements. The “Total Area” measurement was used to calculate the average total degradation per image per coverslip. Data are the mean ± standard deviation of three, independent experiments.

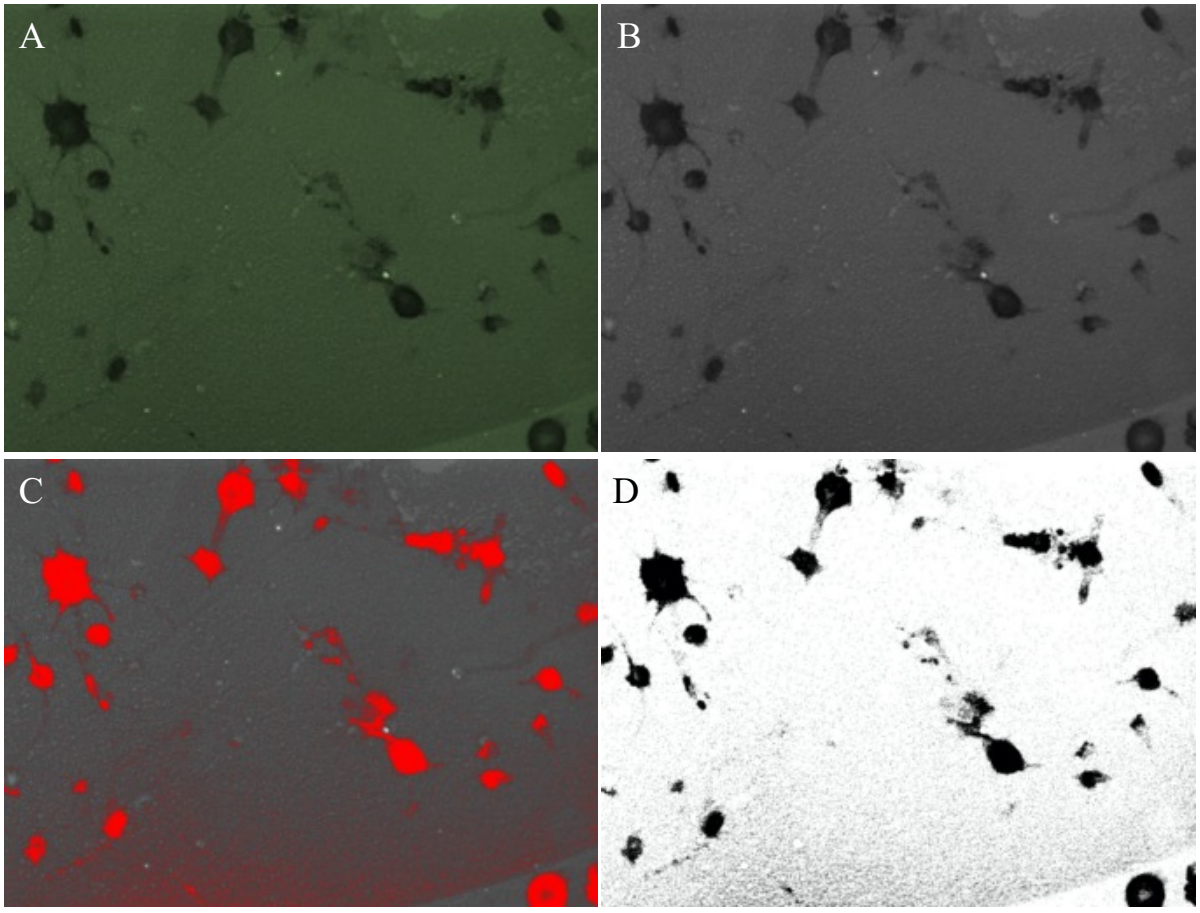

FIG 1 Gelatin Degradation Image Processing. Raw images of gelatin degradation were collected (A) and imported into ImageJ software where they were converted to 8-bit format (B) for processing through ImageJ particle analysis algorithm. The image threshold was then adjusted to account for black spots where degradation had occurred (C), displayed by the software in red. After the threshold for degradation had been set, all other pixels excluded by the threshold process were set to white (D) and all black pixels that were in a group greater than 10 square pixels in size were counted via particle analysis.

mRNA Collection and Reverse Transcription

To generate cDNA from mRNA in preparation for examining gene expression among known podosome transcripts and macrophage markers, THP-1 or primary monocytes were polarized to macrophage subtypes using previously described methods at a concentration of 1 x 10^6 cells/well in a 6-well dish. The macrophages were then infected with or without (mock) rwt or rM51R-M virus at an MOI of 1 or 10 pfu/cell for 12 hours. Post-infection, the dish was placed on ice, the media was removed, and the cells were lysed in 1mL TRIzol reagent (Invitrogen). The solution was pipetted up and down several times to facilitate complete homogenization before incubating for 5 minutes on ice to allow complete dissociation of the nucleoproteins. After incubation, the lysate was transferred to a microfuge tube, 200μL of chloroform (Sigma-Aldrich) was added, and the tube was capped, briefly vortexed, and incubated in a refrigerated microcentrifuge at 4°C for 3 minutes. The samples were then centrifuged at 12,000xg for 15 minutes at 4°C after which the colorless, upper aqueous phase containing the RNA was transferred to a new tube. RNA was precipitated by adding 500 μL of isopropanol, incubating for 10 minutes on ice, and centrifuging at 12,000xg for 15 minutes at 4°C. The supernatant was removed and the RNA pellet was suspended in 1 mL of 75% ethanol in RNase-free water (Fisher Scientific). The sample was briefly vortexed and then centrifuged at 7,500xg for 5 minutes at 4°C. The supernatant was removed and the wash step repeated two more times. After the final wash, the RNA pellet was vacuum dried by opening the tube in the RNase-free PCR workstation for 5 minutes, ensuring that a small layer of liquid remained and that the RNA pellet was not completely dried out. The pellet was then resuspended in 50 μL RNase-free water with 0.1% EDTA (Fisher Scientific). RNA concentration was determined using a NanoDrop 1000 (Thermo Scientific) with NanoDrop

1000 Operating Software version 3.8.1. Total mRNA collection ranged from 2.6 μg to 10.4 μg per sample.

RNA (2 μg) was reverse transcribed to cDNA using the Applied Biosystems High-Capacity cDNA Reverse Transcription Kit (Thermo-Fisher) according to the manufacturer's protocol. Briefly, reverse transcription buffer, random primers, dNTPs, MultiScribe reserve transcriptase, and nuclease-free water were added with RNA to a thin-wall PCR tube for a final volume of 20 μL. The PCR tubes were then placed in an Eppendorf 6331 Nexus Thermocycler that was programed for the following PCR steps: 10 minutes at 25°C, 120 minutes at 37°C, 5 minutes at 85°C, and 10 minutes at 4°C. cDNA concentration was determined using the NanoDrop 1000 and ranged from 1.3 μg to 11.3 μg per sample.

qPCR Primer Generation

The AmiGo2 Gene Ontology Search Database (Gene Ontology Consortium) was used to locate transcripts associated with podosomes and macrophage polarization. A search of NCBI's GenBank located the highest ranked mRNA isoform in *Homo sapiens*. The entire FASTA sequence was analyzed with OligoPerfect Primer Design software (Thermo Fisher) for forward and reverse primers as listed in Table 1.

Protein	Function	Primers (F/R)	Reference
Lymphocyte-Specific Protein 1 **LSP 1**	Actin-binding and cellular defense responses	**F - ACAATACACCCAGGCCATCG** **R - CTTGCTCATGTCTCCAGCCA**	(32)
Matrix Metalloproteinase-14 **MMP-14**	ECM degradation and remodeling, Cytoskeletal reorganization, Cell migration	**F - GTACCCAATTGGCAGCCTCT** **R - TGACTGAGCAACGAAGACCC**	(17)
Hematopoietic Cell Kinase **HCK**	Cell adhesion and migration, Reorganization of actin cytoskeleton, Promotes actin polymerization, Promotes podosome formation	**F – TCCCACATCCACCATCAAGC** **R - GCTGAGGTCTTCGTGGTGAA**	(39)
ARP 2/3 Subunit 1B **ARPC1B**	Mediates actin polymerization, Provides force for cell motility	**F - GAACCTGGACAAGAAGGCGA** **R - GATACTCATGCCGCCATCCA**	(20)
Neural Wiskott-Aldrich Syndrome Protein **N-WASp**	Stimulates the Arp 2/3 complex, Extension and maintenance of podosomes, Positive regulation of clathrin-dependent endocytosis	**F - CCACACAACTCAGGTCCTCC** **R - AGGTGGAGGAGGGTACATCC**	(53)
VSV Nucleoprotein **VSV-N**	Protects viral genome from nucleases, Concomitant with replication	**F - GCAGACGAGCTATGCCAGAT** **R - TTCGATGTCGTCAGGCTGTC**	(102)
Dynamin 2 **DNM2**	Microtubule-associated force-producing protein, Binds and hydrolyzes GTP, Membrane invagination and fission during endocytosis, Positive regulation of podosome	**F - TTCGCCATCTTCAACACGGA** **R - CCCATCCTCGTTTTCTGCCT**	(103)
Cortactin **CTTN**	Actin organization, Cell invasion, Promotion of podosome turnover, Receptor-mediated endocytosis	**F - CGGCCACGAATATCAGTCGA** **R – GTCTTTCTGGGAGGCATGCT**	(104)
Cofilin **CFL1**	F-actin depolymerizing activity	**F – ACAACATCCCCATTCCCCAC** **R - GTGACCAGGGGAAAAGGGAG**	(105)
Tyrosine Kinase Substrate 5 **Tks5**	Scaffolding protein of podosomes, Positive regulator of cell migration	**F - AGCACCCTCTCCTACTCCAG** **R - ATTCTTCCTCCCTCCCTCCC**	(45)
Signal Transducer and Activator of Transcription 1 **STAT-1**	M1 polarization marker, Drives cells into an anti-viral state, Negative regulation of angiogenesis	F -GGCACGCACACAAAAGTGAT R- AGAGGTCGTCTCGAGGTCAA	(1)
Signal Transducer and Activator of Transcription II **STAT-6**	M2 polarization marker, Immunosuppressive cytokine signaling	F – AGATGAGCCTGCCCTTTGAC R - AGGCAGCAGAGGAGGGAATA	(1)
Arginase-I **Arg-1**	M2 polarization marker, Negative regulation of IFN-γ signaling, Negative regulation of T-cell proliferation, Pro-metastatic marker	F – ACGGAAGAATCAGCCTGGTG R - CCTGGCACATCGGGAATCTT	(1)
Major Histocompatibility Complex Class II **MHC-II**	M1 polarization marker, Essential for HLA class II promoter, Pro-inflammatory response	F – GCTCACGGGACTCTATGTCG R - CAGGAAGCATTGCAGGAGGA	(1)
Glyceraldehyde 3-Phosphate Dehydrogenase **GAPDH**	Housekeeping gene involved in glycolysis	F - TGCTGCATTCGCCCTCTTAA R - GCGCCCAATACGACCAAATC	(106)

TABLE 1 qPCR Primers. Forward and reverse primers and function of the genes/proteins of interest. All primers were designed using ThermoFisher OligoPerfect design software after searching for podosome and macrophage polarization transcripts in AmiGo2 and locating the FASTA sequence in GenBank.

qPCR Gene Expression Assay

To quantitate transcripts relative to GAPDH, qPCR was conducted utilizing 100 ng cDNA along with 1 μL of 5 μM Forward Primer, 1 μL of 5 μM Reverse Primer, 10 μL igScript SYBR Green qPCR 2X Master Mix (Intact Genomics) and enough RNase/DNase-free water to bring the sample to a total volume of 20 μL all on ice in a 96-well optical plate (Applied Biosystems). The plate was sealed using MicroAmp Optical Adhesive Film (Thermo Fisher Scientific), inserted into an Applied Biosystems 7500 Real-Time PCR System, and programed using Applied Biosystems 7500 v2.x software. PCR cycling conditions were set for a 15-minute initial denaturation cycle at 95°C, 40 cycles of denaturation at 95°C for 5 seconds and annealing/extension at 60°C for 30 seconds, and a final melting curve analysis. Control amplification for the housekeeping gene GAPDH was performed in all samples. Following the amplification, the same threshold was set to compare Ct values derived from different experiments. The mean Ct values from each sample were normalized against the corresponding GAPDH Ct values (ΔC_t analysis) was calculated as $Ct_{Experimental\ Gene}/Ct_{GAPDH}$. The normalized data from VSV-infected cells were compared with the normalized macrophage phenotype value and the abundance of the experimental gene expression in the samples were expressed as relative percentages of macrophage phenotype, referred to as a $\Delta\Delta\ C_t$ analysis, calculated as ($\Delta\ Ct_{Gene\ of\ Interest}$ / $\Delta\ Ct_{Phenotypic\ Mock}$).

VSV Replication in Primary Macrophages

To examine the ability of VSV to replicate in primary macrophages, PBMCs were first seeded in a 6-well plate at a concentration of 1 x 10^6 cells/well before being polarized to

the different macrophage subtypes using previously described methods. Macrophages were infected with rwt-GFP or rM51R-GFP viruses at MOIs of 1 or 10 pfu/cell for 12 hours. Live images of the cells were taken on the previously described Olympus IX81 microscope at 20x magnification and analyzed with cellSens Dimension software. A total of 10 images per condition per experiment were analyzed. The percentage of GFP-positive cells was determined using the ImageJ 1.8.0 software counting tool. Data are the mean ± the standard deviation of three independent experiments.

Measurement of Cell Viability

The viability of primary macrophages in response to VSV infection was determined using an MTT assay (Cell Proliferation Kit I (MTT); Roche Diagnostics). To examine viability, isolated PBMCs were seeded into 96-well plates at 1 x 10^5 cells/well and polarized to M1 or M2 macrophages using previously described methods. Cells were infected with or without (mock) rwt or rM51R-M viruses at MOIs of 1 or 10 pfu/cell for 12 and 24 hours before being assayed for viability according to the manufacturer's directions. Briefly, after the infection period, an MTT labeling reagent was added to each well and cells were incubated for 4 hours. The MTT reagent is converted from its yellow liquid state to a purple crystalized formazan salt via metabolic reactions in the mitochondria of viable cells. At the end of the incubation period, solubilization buffer was added to each well, causing the crystalized purple salt to dissolve into solution. The microplate was then placed back into the incubator for 12 hours before being read using a SpectraMax Plus 384 (Molecular Devices) microplate reader at an absorbance reading at 550 nm and using a reference wavelength at 650 nm. Data are the mean ± standard deviation from three, independent experiments with

each sample performed in triplicate. All data were normalized to mock-infected conditions for each macrophage subtype at 12 or 24 hours.

Cell Lysates

Primary PBMCs were seeded in a 6-well plate at a concentration of 1 x 10^6 cells/well. Polarized macrophage subtypes were generated using previously described methods while monocytes were left untreated. All cells were washed with 1 mL of ice-cold 1 mM sodium orthovanadate in PBS, then lysed using 100 µL of lysis buffer composed of 20 mM HEPES (pH = 7.00), 110 mM sodium chloride, 40 mM sodium fluoride, 1% NP40, 1 mM sodium orthovanadate, 10 µg/mL aprotinin, 10 µg/mL benzamidine, 10 µg/mL leupeptin, 10 µg/mL pepstatin, 2 mM DTT, and 1 mM PMSF/DMSO. The cells were scraped from the plates on a bed of ice, transferred to ice-cold microfuge tubes, incubated for 10 minutes on ice, and the cellular debris removed by centrifugation at 10,000xg for 10 minutes at 4°C. Protein concentrations in the supernatants were determined using a detergent-compatible protein assay kit (Bio-Rad) according to the manufacturer's instructions against a series of BSA standards.

SDS-PAGE/Immunoblotting

For SDS-PAGE/immunoblot analysis, 10 µg of whole cell lysate protein were denatured in SDS-containing sample buffer and heated to 95°C for 10 minutes before loading on a 10% polyacrylamide gel (Bio-Rad). Proteins were separated at 125 V for 60 minutes, and then transferred under wet conditions to a 0.45 µm nitrocellulose membrane (Bio-Rad) at 100 V for 1 hour. After transfer, the blot was blocked in PBS containing 1% Tween-20

(PBST) containing 5% milk and 1% BSA for at least one hour at room temperature. After blocking, the membrane was incubated with a primary antibody specific to CD204 (1:500; Santa Cruz; #sc-166184), pSTAT1 (Y701) (1:1000; Cell Signaling; #9167S), STAT1 (1:1000; Cell Signaling; #9172S), or GAPDH (1:1000; Cell Signaling; #2118) in the previously described blocking solution for overnight at 4°C. After several washes in PBST, this was followed by incubation in a species-specific peroxidase-conjugated secondary antibody (1:2000, Cell Signaling, #7074/mouse or Cell Signaling, #7076/rabbit) in blocking solution for 1 hour at room temperature. After several washes in PBST, proteins were visualized using SuperSignal West Dura Extended Duration Substrate (Thermo Fisher Scientific) and a ChemiDoc XRS+ imager and Image Lab 6.1 software (Bio-Rad). Data are the result of one experiment.

Podosome Formation

To analyze podosome formation, PBMCs were plated onto sterile glass coverslips in 6-well dishes at 1 x 10^6 cells/well before polarizing to M1 or M2 macrophages using previously described methods. Cells were infected with or without (mock) rwt-GFP or rM51R-GFP viruses at MOIs of 1 or 10 pfu/cell for 12 hours. The macrophages were then fixed in 3% formaldehyde and permeabilized in 0.4% Triton X-100 as described previously before staining with 0.5% Texas Red-X phalloidin in 5% donkey serum/PBS (MilliporeSigma) for 2 hours at room temperature in the dark. Coverslips were mounted onto glass slides in ProLong Gold Antifade Mounting Media with DAPI, cured in the dark overnight, sealed with nail polish, and imaged by fluorescence microscopy as previously described. Each coverslip was imaged under type F immersion oil (Olympus) using the

Olympus IX81 microscope at 100x magnification. Ten random images were collected for each experimental condition. The number of podosomes in each cell was quantified using ImageJ 1.8.0 software and then normalized to mock-infected cells. Podosome incidence (the percentage of cells with any number of podosomes) and multiplicity (the number of podosomes/cell) was determined for each sample group. Data are the mean ± standard deviation of three, independent experiments.

Statistical Analysis

All statistical analysis tests were carried out using Minitab Data Analysis software version 20.2. Normal distribution for each condition was confirmed via Anderson-Darling normality test using Minitab software. The alpha value for all tests was 0.05. All assay statistics except for podosome multiplicity were the mean value of three independent experiments and were analyzed for significance using an independent unpaired Students' T-test for equal sample size and variance. Prior to t-test calculations, an f-test was used to determine if variances of compared conditions were equal.

Podosome Multiplicity

Individual cells were analyzed for the number of podosomes using ImageJ software, as previously described. Cells were analyzed via one-way ANOVA, as it was determined that each cell was an independent sample of the population of the condition in question. Pairwise comparisons were made using Tukey's Honest Significant Difference (HSD) test.

CHAPTER 3: RESULTS

M2 THP-1 Macrophage Podosome Multiplicity Exceeds that of M1 Macrophages and is Sensitive to Infection with rwt Virus

A previous study in the Ahmed and Seals laboratories investigated the effects of oncolytic VSV strains on THP-1 macrophages with specific focus on their potential abilities to coerce M2 macrophages to an M1-like phenotype (64). As part of that study, we investigated the impact of rwt-GFP or rM51R-GFP viruses on macrophage podosome development. M0 macrophages, which are similar to tissue resident macrophages of the innate immune system, were also tested. Macrophages form podosomes that are easily visualized by fluorescent microscopy as punctate F-actin structures (FIG 2). Based on the presence of these F-actin puncta, our experiments indicated that both M0, M1, and M2 THP-1 macrophages formed podosomes (FIGs 2A, 2B, and 2C, respectively), but they each displayed differences in the average number of podosomes per cell (FIG 2J). Specifically, M0 and M2 macrophages made nearly twice as many podosomes (~92-116/cell) than the M1 subtype (~51/cell). Importantly, following infection of M2 macrophages with rwt virus, we observed a significant reduction in the average number of podosomes relative to mock-infected cells, a difference of close to 1.5-fold at an MOI of 10 pfu/cell. There was also a trending decrease in podosome number in rM51R-M virus-infected M2 macrophages, but these data were not significant from the mock-infected cells. In contrast, M1 THP-1 macrophages were generally unaffected by VSV (FIG 2J). That is, while we observed a significant decrease in the number of podosomes after infection of M1 macrophages with rwt virus at an MOI of 1 pfu/cell, there were no statistical differences in podosome numbers

relative to the mock-infected condition when cells were infected with rwt virus at the higher MOI of 10 pfu/cell nor with rM51R-M virus at either MOI. These results indicate that M2 macrophages are more susceptible than M1 macrophages to VSV-induced changes in podosome multiplicity. Interestingly, M0 macrophage podosomes were also significantly reduced following infection with both rwt and rM51R-M viruses, but subsequent studies focused on dissecting the differences between the M1 and M2 macrophage populations.

M1 THP-1 Macrophage Podosomes Initially Degrade more Gelatin than M2 Macrophages

Although the data in FIG 2 provides insight into the innate differences in podosome numbers among macrophage subtypes as well as the impact of VSV strains thereof, it does not inform on the most prominent function of macrophage podosomes in degrading ECM proteins through the clustered proteolytic activity of MMPs. Such podosome activity can be measured through an *in situ* zymography assay. For this assay, porcine gelatin was used as a surrogate for the ECM secreted by fibroblasts and other cells within tissues, and which is normally degraded by macrophages as part of their professionally invasive behavior. The gelatin was conjugated with FITC to easily visualize areas of degradation through fluorescent microscopy. As seen in representative images of a time-course of gelatin degradation by M1 and M2 THP-1 macrophages, the FITC-conjugated gelatin monolayer revealed areas of gelatin clearance as shown by the presence of black spots or larger areas of blackness of nearly the same size as the cells (FIG 3).

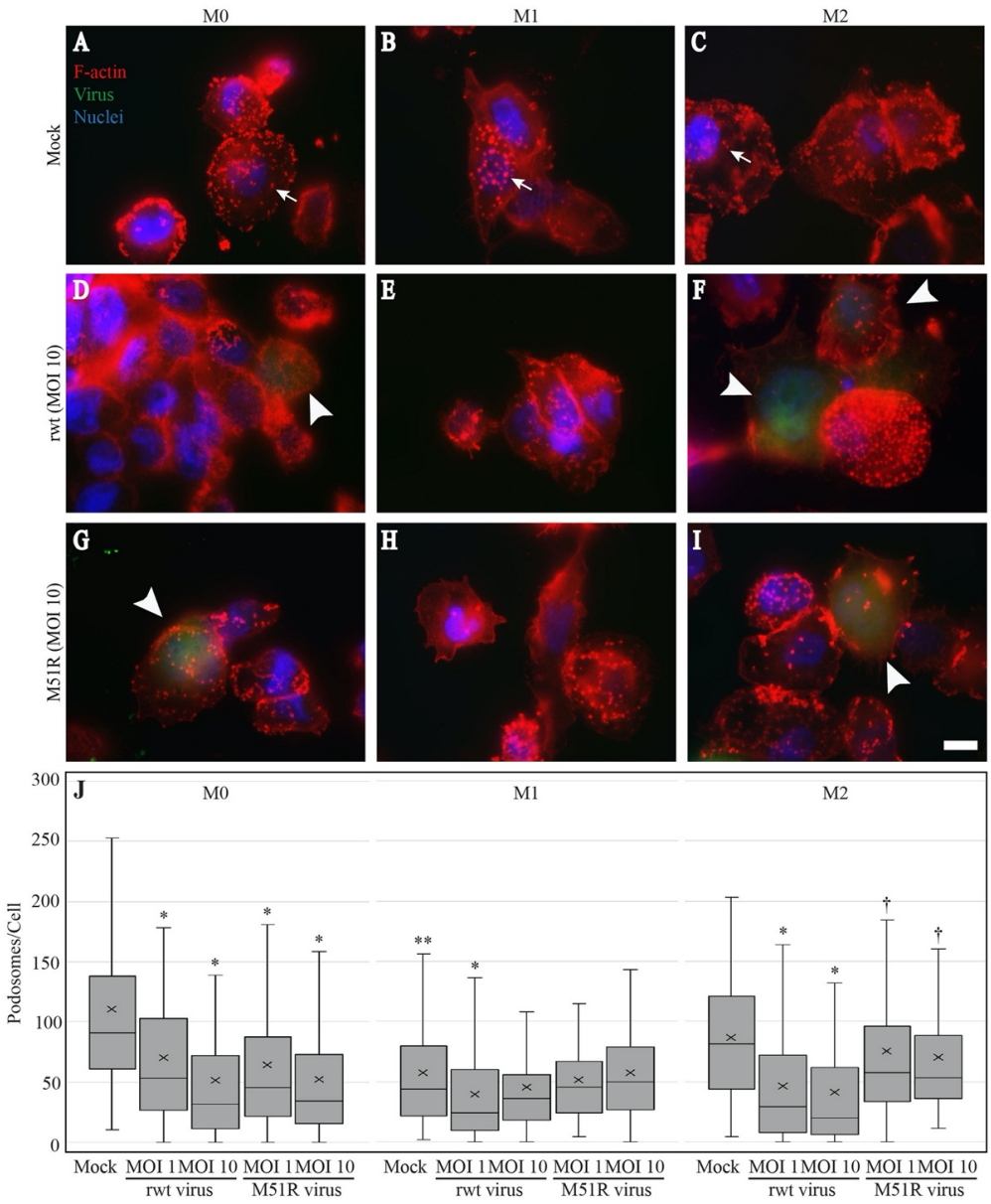

FIG 2 Differences in Podosome Multiplicity in THP-1 Macrophage Populations With or Without VSV Infection. Representative fluorescent images of M0 (A, D, and G), M1 (B, E, and H), and M2 (C, F, and I) THP-1 macrophages at 12 hours post-infection with or without (mock) rwt and rM51R-M viruses at an MOI of 10 pfu/cell. Formaldehyde-fixed cells were stained with Texas Red-X phalloidin (Life Technologies) to visualize F-actin-rich podosomes (arrows). Nuclei (blue) were stained with DAPI. Cells with active viral replication (green) are indicated with arrowheads. (J) Ten, random images containing a range of cells (48 -107 per experimental condition) were used to count podosome numbers per cell. Box plots, where 'X' is the mean, show the collective results of four, independent experiments. Statistical analyses were conducted using a one-way ANOVA with post-hoc Tukey HSD test. * represents statistical differences between mock and viral infections. ** represents statistical differences between M0, M1, and M2 macrophages under mock conditions. † represents statistical differences between rwt and rM51R-M viruses at the indicated MOI.

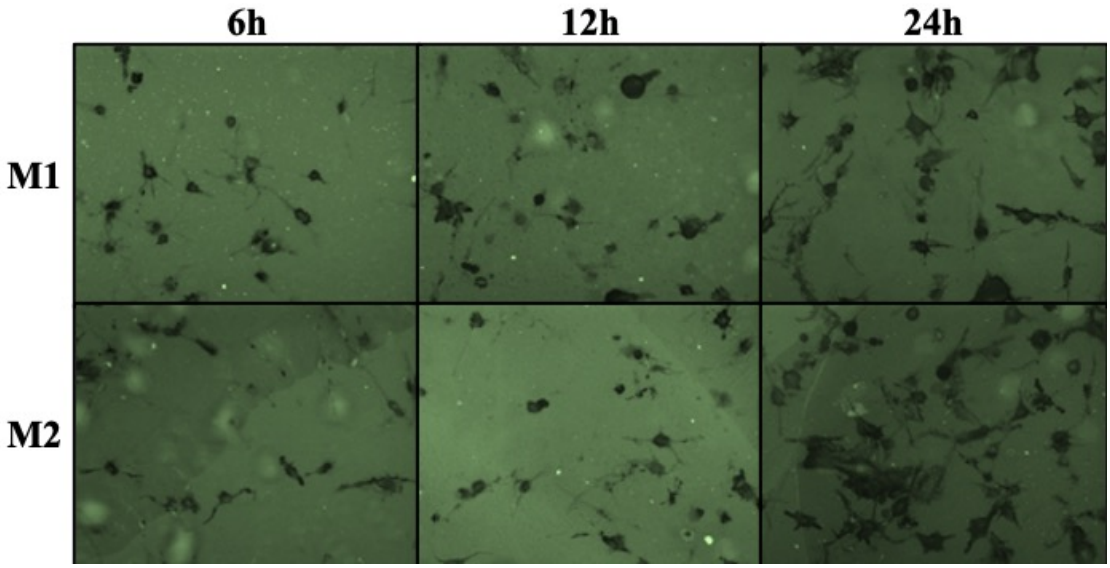

FIG 3 Images of Podosome Activity in M1 and M2 THP-1 Macrophages. Representative fluorescent images of M1 (top row) and M2 (bottom) THP-1 macrophage-mediated degradation of gelatin at 6, 12, and 24 hours (h). FITC-conjugated porcine gelatin is represented in green and gelatin degradation represented in black.

The total area of degradation by each macrophage subtype at each timepoint was measured with ImageJ and is shown as a total pixel count (FIG 4). M1 macrophages degraded significantly more gelatin than their M2 macrophage counterparts at 6 and 12 hours, by 30% and 15% respectively. However, by the 24-hour timepoint, there was no difference between the two macrophage subtypes. Interestingly, degradation by M2 macrophages continued to significantly increase over time, with a 20% increase from 12 to 24 hours. M1 macrophages reached a maximum level of gelatin degradation by the 6-hour timepoint. These data indicate a similar competency between M1 and M2 THP-1 macrophages when it comes to gelatin degradation activity, though M1 macrophages appear to be able to initially degrade the gelatin at a faster rate. It also suggests that while M2 macrophages produce more podosomes than M1 macrophages (FIG 2), their ability to degrade gelatin may initially be lower (FIG 4).

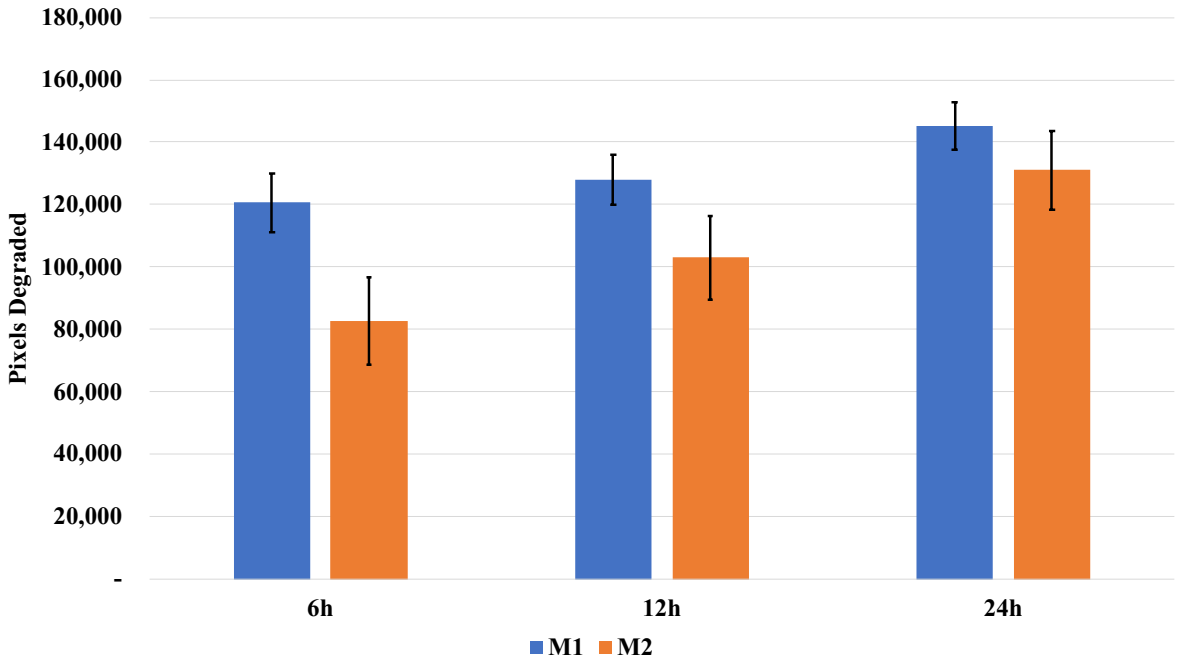

FIG 4 Differences in Podosome Activity in M1 and M2 THP-1 Macrophages. Ten, random images were used to determine the total area of gelatin degradation in M1 and M2 THP-1 macrophages plated on FITC-conjugated porcine gelatin at 6, 12, and 24 hours (h). Results are the average and standard deviation of three, independent experiments. Statistical analyses were conducted using a Student's t-test with significance determined at $p < 0.05$. * represents statistical differences between M1 and M2 macrophages at the same timepoint. ◊ represents statistical differences between the same macrophage subtype at different timepoints.

VSV Exerts Differential Effects on Podosome Activity in M1 and M2 THP-1 Macrophages

After elucidating the podosome-associated gelatin degradation activity of M1 and M2 THP-1 macrophages, we next examined the impact of rwt and rM51R-M viruses. We hypothesized that because infection of M1 macrophages with both strains of VSV did not alter podosome number, gelatin degradation would also not be impacted. Nevertheless, our results showed that the both strains of VSV at both MOIs initially negatively impacted gelatin degradation by podosomes in M1 macrophages, with a 20-30% decrease in degradation relative to mock-infected cells at 6 hours post-infection (FIG 5A). This effect was short-lived following infection with rwt virus as the M1 macrophages rapidly recovered

their ability to degrade gelatin to levels seen under mock conditions by the 12- and 24-hour timepoints. rM51R-M virus-infected M1 macrophages also increased their gelatin-degrading podosome activity over time, but in contrast to rwt virus-infected cells, the levels of degradation remained significantly lower than mock conditions at both 12 and 24 hours. Recalling that M2 THP-1 macrophage podosome multiplicity declined following infection with rwt virus (FIG 2), we hypothesized a similar result for podosome activity. Degradation by M2 macrophages, however, was not affected by both rwt and rM51R-M viruses at any MOI (FIG 5B).

So collectively we have seen some surprising differences in the podosomes of these macrophage subtypes and how they are impacted by VSV infection. M1 THP-1 macrophages develop fewer podosomes, but they have the capability of degrading the ECM faster than their M2 macrophage counterparts. And in terms of how they respond to VSV, M1 macrophage podosomes are primarily compromised in their gelatinolytic activity by rM51R-M virus while M2 macrophages are primarily compromised in terms of podosome numbers by rwt virus.

Gene Expression Profiles Differ Between M1 and M2 THP-1 Macrophages

In an attempt to dissect the mechanisms by which M1 and M2 THP-1 macrophages modulate podosome development following infection with VSV, we determined the expression profile of podosome-associated genes under mock- and virus-infected conditions. Although M2 macrophages were shown to degrade significantly less ECM than M1 macrophages at early timepoints, they have significantly greater numbers of podosomes.

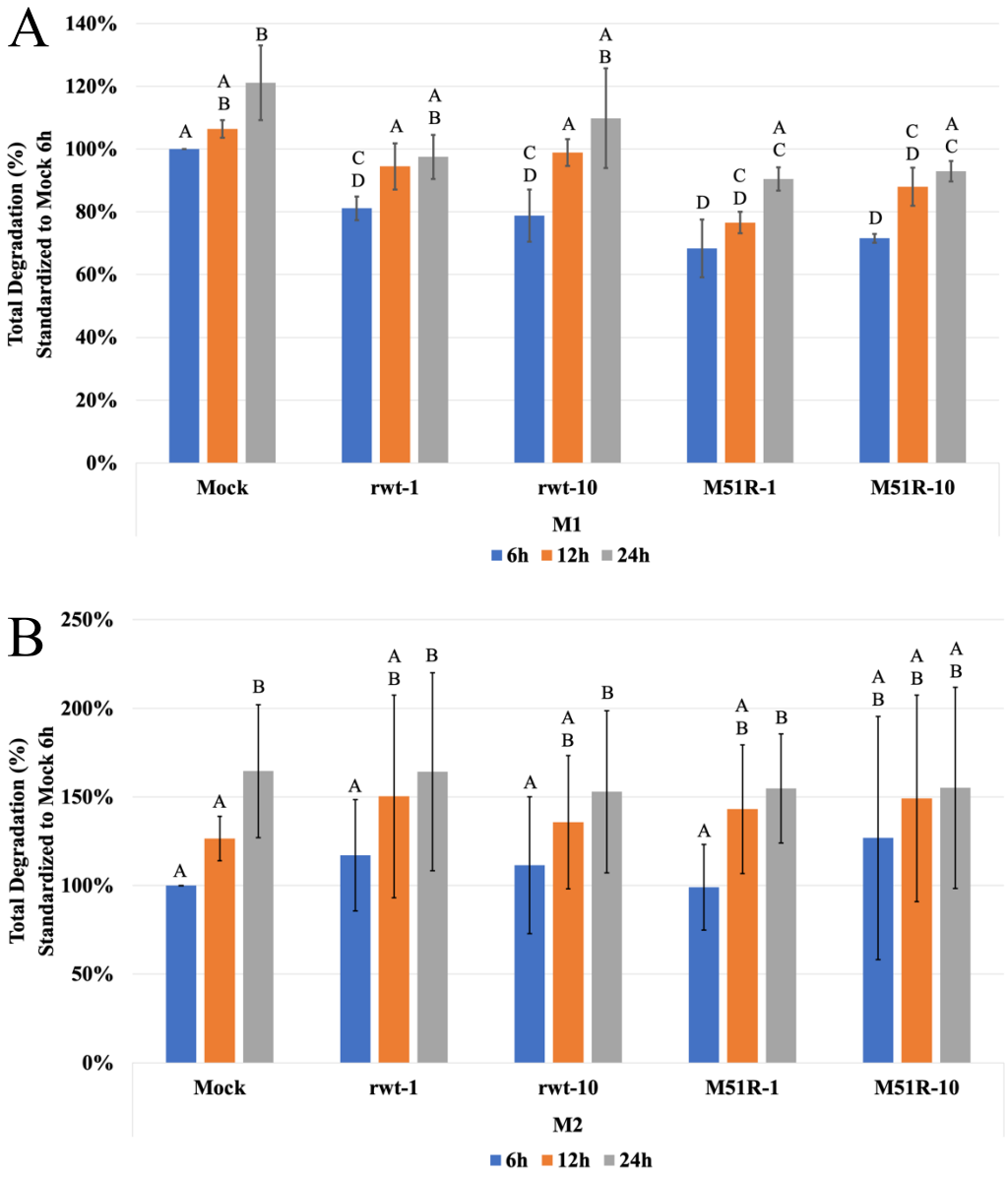

FIG 5 Differences in Podosome Activity in M1 and M2 THP-1 Macrophages With or Without VSV Infection. M1 (A) and M2 (B) THP-1 macrophages were infected with or without (mock) rwt or rM51R-M virus at an MOI of 1 or 10 pfu/cell. Ten, random images were used to determine the total area of gelatin degradation at 6, 12, and 24 hours (h) post-infection. Results are the average and standard deviation of three, independent experiments normalized to the degradation seen under mock conditions at 6 hours. Statistical analyses were conducted using a Student's t-test with significance determined at $p < 0.05$. Statistical differences between conditions and timepoints are noted with differing letters.

We therefore hypothesized that M2 macrophages would express higher amounts of podosome-associated transcripts than M1 macrophages. To test this hypothesis, mRNA from mock-infected M1 and M2 THP-1 macrophages was collected and reverse transcribed to cDNA. The cDNA was then added to a Sybr Green Master Mix solution along with confirmed primers for the genes of interest and subjected to quantitative real-time PCR (qRT-PCR). Initial results were reported as the point when the transcript of interest reached threshold (C_t). These C_t values were then compared to the C_t values of the housekeeping gene GAPDH to generate ΔC_t values (TABLE 6). Finally, the ΔC_t value of each gene in M2 macrophages was divided by the ΔC_t value of the same gene in M1 macrophages to generate $\Delta\Delta C_t$ ratios.

Generally, the polarization of THP-1 macrophages was associated with higher transcript levels for most analyzed genes relative to the housekeeping gene GAPDH; *i.e.* ΔC_t values greater than 1 (TABLE 6). Only STAT1 was down-regulated relative to GAPDH in this data set, though none of these differences were statistically evaluated. M2 macrophages did express significantly greater transcript levels for the actin nucleation protein N-WASP, the actin depolymerization protein cofilin, and the podosome stabilization protein dynamin 2 than M1 macrophages; *i.e.* $\Delta\Delta C_t$ values significantly greater than 1 (TABLE 6). The actin regulatory kinase Hck was also upregulated, but the differences were not statistically significant. While these data may be consistent with the increased number of podosomes observed in M2 macrophages, other transcripts for the actin nucleation protein cortactin and the matrix degradation protein MMP-14 were more prominent in M1 macrophages; *i.e.* $\Delta\Delta C_t$ values significantly less than 1. The increase in MMP-14 in M1 macrophages might explain the faster rate of podosome-associated gelatin degradation seen in this subtype (FIG 4). The

M1 polarization marker MHC-II was also expressed at higher levels by M1 macrophages as expected, but so was the M2 macrophage marker STAT-6. We recognize that transcript levels may not necessarily equate to the protein levels of these polarization markers. Conversely, we also recognize that these changes in polarization markers may reflect the wide range of phenotypes that are known to exist in macrophage populations *in vivo*.

Function	Gene	M1	M2	Ratio (M2/M1)
Actin Polymerization Promotion	**HCK**	2.66	3.92	1.47
Actin Nucleation	**ARP 2/3**	25.19	19.23	0.76
	Cortactin	2.55	1.83	0.72*
	N-WASP	6.75	15.67	2.32*
Podosome Structure	**Tks5**	57.88	57.48	0.99
Degradation	**MMP-14**	14.17	9.99	0.71*
Podosome Stabilization	**Dyn 2**	17.51	2154.79	123.06*
	LSP-1	14.47	11.31	0.78
Actin Depolymerization	**Cofilin**	20.25	30.48	1.51*
M1 Marker	**MHC-II**	6.39	4.47	0.70*
	STAT-1	0.49	0.49	1.00
M2 Marker	**ARG-1**	8.94	7.7	0.86
	STAT-6	7.7	3.29	0.43*

TABLE 2 Differences in Selected Podosome- and Polarization-associated Transcripts in M1 and M2 THP-1 Macrophages. M1 and M2 THP-1 macrophages were lysed in TRIzol reagent and the isolated mRNA transcripts were reverse transcribed to cDNA and amplified in a SYBR Green Master Mix with selected primers by qRT-PCR. The ΔC_t values of each gene of interest are shown for M1 and M2 macrophages relative to GAPDH. The ratio is a $\Delta\Delta C_t$ measurement whereby the ΔC_t of the M2 macrophage transcript of interest was divided by the ΔC_t of the same transcript in M1 macrophages. Results are the average of three, independent experiments. Statistical analyses were conducted using a Student's t-test with significance determined at $p < 0.05$. * represents statistical differences between M1 and M2 macrophages. Heat map colors were generated using the logarithm of the M2/M1 ratio.

VSV Exerts Differential Effects on Podosome- and Polarization-associated Gene Expression in M1 and M2 THP-1 Macrophages

The fidelity of measuring gene expression changes following VSV infection was determined by monitoring a viral transcript. Following infection of M1 and M2 THP-1

macrophages with rwt or rM51R-M virus at MOIs of 1 or 10 pfu/cell, we observed statistically significant increases in transcripts for the VSV N protein. The increases ranged from 1.59 to 4.92-fold for M1 macrophages (TABLE 3A) and from 3.48 to 13.22-fold for M2 macrophages (TABLE 3B). The higher levels of N protein transcripts in M2 versus M1 macrophages might be consistent with the greater susceptibility of M2 THP-1 macrophages to infection and replication by VSV (64).

Next we analyzed any changes in the transcripts for M1 and M2 polarization markers, keeping in mind that prior data had suggested an upregulation of M1 markers when M2 macrophages were infected with rM51R-M virus (64). When M1 macrophages were investigated, there was either significant upregulation of the M1 transcripts MHC-II and STAT-1 in response to both viral strains at an MOI of 1 pfu/cell or no significant change at the higher MOI of 10 pfu/cell (TABLE 3A). This was complemented by lower transcript levels for the M2 markers ARG-1 and STAT-6, but only at an MOI of 10 pfu/cell. In contrast, M2 THP-1 macrophages demonstrated a remarkable upregulation of polarization markers association with both M1 and M2 macrophages. Consistent with the previously hypothesized M2-to-M1 repolarization of macrophages by rM51R virus, there was an upregulation of the M1 transcript MHC-II (TABLE 3B). The caveat to this, however, was that (i) MHC-II transcripts were also increased by rwt infection, (ii) transcript levels for the M1 marker STAT-1 were unaffected or even down-regulated by rM51R-M virus at an MOI of 10 pfu/cell, and (iii) transcript levels for the M2 markers ARG-1 and STAT-6 were upregulated in response to both viral strains at both MOIs (TABLE 3B).

A

Function	Gene	rwt-1	rwt-10	M51R-1	M51R-10
Viral Load	**VSV N**	2.79*	1.87*	4.92*	1.59*
Actin Polymerization Promotion	**HCK**	1.62*	0.90	5.78*	1.72
Actin Nucleation	**ARP 2/3**	2.11*	1.22*	3.38*	1.86*
	Cortactin	0.90	0.85	0.73	0.52*
	N-WASP	0.89	0.56	11.75*	6.39*
Podosome Structure	**Tks5**	1.11	0.52*	1.78*	0.83
Degradation	**MMP-14**	1.69	0.59*	3.33*	0.67
Podosome Stabilization	**Dyn 2**	0.38*	0.55*	3.48*	2.16*
	LSP-1	1.98*	1.16	3.06*	1.19
Actin Depolymerization	**Cofilin**	2.50*	0.94	1.46*	0.28*
M1 Marker	**MHC-II**	1.77*	0.84	1.55*	0.78
	STAT-1	1.20	0.93	1.60*	0.74
M2 Marker	**ARG-1**	1.17	0.71*	1.38	0.79*
	STAT-6	0.98	0.78*	0.62*	0.31*

B

Function	Gene	rwt-1	rwt-10	M51R-1	M51R-10
Viral Load	**VSV N**	3.48*	12.34*	13.22*	8.22*
Actin Polymerization Promotion	**HCK**	7.24	885.29*	4.14	837.24*
Actin Nucleation	**ARP 2/3**	21.26*	77.98*	96.00*	48.17*
	Cortactin	0.96	1.74	2.97	8.31*
	N-WASP	14.03	59.92*	64.45*	21.19*
Podosome Structure	**Tks5**	6.32*	16.80*	13.78*	6.68*
Degradation	**MMP-14**	4.14	18.83*	7.04	4.48
Podosome Stabilization	**Dyn 2**	0.18*	0.57*	0.57*	0.44*
	LSP-1	2.60	10.93	42.52*	22.09*
Actin Depolymerization	**Cofilin**	0.65	1.54	8.00*	0.41
M1 Marker	**MHC-II**	5.17*	22.78*	19.77*	9.32*
	STAT-1	0.92	1.48	1.20	0.33*
M2 Marker	**ARG-1**	5.28*	18.32*	17.94*	13.83*
	STAT-6	4.17*	13.45*	8.11*	5.92*

TABLE 3 Differences in Selected Podosome- and Polarization-associated Transcripts in M1 and M2 THP-1 Macrophages With or Without VSV Infection. M1 (A) and M2 (B) THP-1 macrophages were infected with or without (mock) rwt or rM51R-M virus for 12 hours at an MOI of 1 or 10 pfu/cell. Cells were processed for qRT-PCR analysis as described in TABLE 6. Displayed are the $\Delta\Delta C_t$ analyses comparing each of the VSV-infected conditions to the mock condition for each gene of interest. Results are the average of three, independent experiments. Statistical analyses were conducted using a Student's t-test with significance determined at $p < 0.05$. * represents statistical differences between VSV-infected and mock-infected cells. Heat map colors were generated using the logarithm of the VSV-infected/mock-infected ratio.

In sum, the data suggested that viral infection was not changing the polarization status of M1 macrophages based on the polarization transcripts analyzed. There was also some evidence of repolarization of M2 macrophages to an M1-like phenotype; however, the data may also suggest a more hybridized macrophage phenotype following infection of M2 macrophages with VSV.

We know that podosome multiplicity is higher in M2 THP-1 macrophages than their M1 counterparts, but infection with rwt virus can reduce podosome numbers (FIG 2). M1 macrophages, on the other hand, more quickly exhibit podosome-associated gelatin degradation activity than M2 macrophages but are also susceptible to the effects of rM51R virus (FIG 5). Given these results, we determined how podosome-associated transcripts might respond to VSV infection and a few observations follow. (1) M2 macrophages nearly universally upregulated podosome transcripts following VSV infection (TABLE 3B) while M1 macrophages either (i) upregulated podosome transcripts, but at far lower levels (usually to rM51R-M virus at an MOI of 1 pfu/cell) or (ii) downregulated podosome transcripts (usually to rwt virus at an MOI of 10 pfu/cell) (TABLE 3A). These down-regulated podosome transcripts in M1 macrophages included dynamin 2, MMP-14, cortactin, and cofilin (TABLE 3A). The only down-regulated podosome transcript in M2 macrophages was dynamin 2, and this occurred in response to both viral strains at both MOIs (TABLE 3B). (2) Transcripts for the Src family kinase member Hck were extremely upregulated (>800-fold) in M2 macrophages, but specifically to both viral strains at the higher viral load of 10 pfu/cell (TABLE 3B). As Hck would be expected to exert pleiotropic effects on cells through its phosphorylation of substrates, its remarkable upregulation here warrants additional studies for validation and testing. (3) There was an upregulation of Arp 2/3 and N-WASp in M2

macrophages to both viral strains at both MOIs suggesting increased actin polymerization following viral infection (TABLE 3B). It is unclear where such polymerization may actually be occurring and whether that has any impact on the number of podosomes in M2 macrophages, though that can be compromised by viral infection. It had been hypothesized that rwt virus, by virtue of its ability to down-regulate host gene expression, might more likely impact podosome markers in M2 macrophages; however, the consistent trend of upregulated actin nucleators and podosome structural genes suggests that any impact of VSV on podosome development may not be due to a general suppression of podosome-associated gene expression (TABLE 3B).

PBMC-derived Macrophages can be Polarized to M1 and M2 Subtypes

THP-1 cells have long been used to study macrophage and dendritic cell populations because of its convenience as a cell line (107). However, because they are derived from the peripheral blood of a monocytic leukemia patient, there are genetic alterations that can affect the physiological characteristics of these cells relative to primary peripheral blood mononuclear cells (PBMCs). Primary cells provide an additional level of insight into the working of physiologically 'normal' macrophages and based on that rationale we sought to determine whether PBMC-derived M1 and M2 macrophage populations developed podosomes and responded to VSV strains in a manner similar to or different from that observed in THP-1-derived macrophages. PBMCs, collected from healthy subjects, were polarized to M1 and M2 macrophage populations using the same types and concentrations of cytokines as described for THP-1 macrophages with the exception that the primary macrophages were differentiated with M-CSF, not the PMA used for THP-1 cells.

Phenotypes were confirmed through immunoblot analysis with antibodies for the M1 marker pSTAT-1 and the M2 marker CD204 (FIG 6). We expected low levels of CD204 expression in PBMCs, isolated monocytes, and M1 polarized macrophages, and higher levels in M2 macrophages. Intermediate levels were expected in CSF-1-differentiated macrophages (Mac). In contrast, M1 macrophages normally express high levels of pSTAT-1. All cells should express STAT-1 and the control protein GAPDH. All of these expectations were true here, and they were all consistent with previous observations in THP-1 macrophages (64). These results therefore establish that the model is both working as hypothesized and that data obtained from primary cells can be compared to those presented previously from THP-1-derived macrophages.

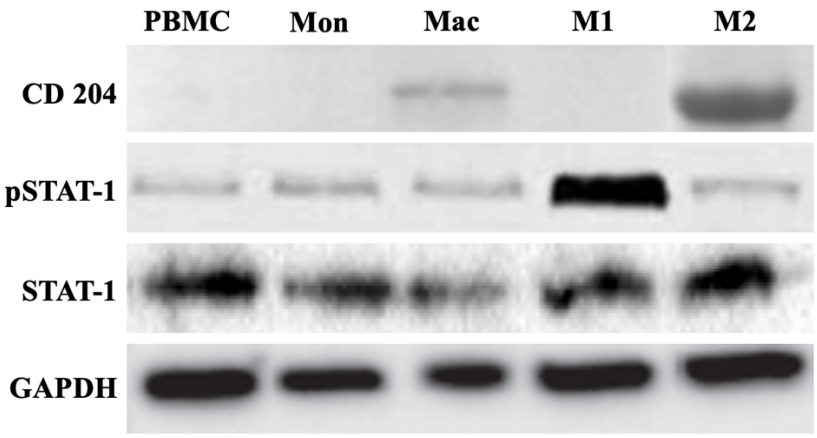

FIG 6 Polarization Marker Status in Primary PBMCs, Monocytes, and Macrophage Populations. Lysates were generated following peripheral mononuclear blood cell (PBMC) isolation, in monocytes after 24 hours of cell culture (Mon), after a 48-hour differentiation period with M-CSF (Mac), and after another 48-hour polarization period to achieve M1 or M2 macrophage subtypes. Proteins were separated by SDS-PAGE, electroblotted to nitrocellulose membranes, and probed with antibodies to CD204, pSTAT-1, total STAT-1, and GAPDH.

PBMC-derived M2 Macrophages are More Susceptible to VSV Infection than M1 Macrophages

Prior to determining the effects of VSV on podosome development, we assessed the ability of VSV strains to replicate within PBMC-derived M1 and M2 macrophages. For this study, cells were infected with rwt-GFP or rM51R-GFP virus for 12 hours. As these viruses enter cells and initiate replication of viral genes, GFP is expressed and can be detected under the FITC channel by fluorescent microscopy (FIG 7). When the percentage of GFP-positive cells was quantitated (FIG 8), the results showed that M1 macrophages were more resistant to infection by both viruses (10-20% GFP-positive) as compared to M2 macrophages (60-75% GFP-positive). These results are consistent with that observed in THP-1 macrophages, though the primary cells were generally more sensitive to VSV infection among these two model systems. That is, no GFP-positive cells were found in M1 THP-1 macrophages compared to 10-36% of the M2 THP-1 macrophages (64). These data do vary, but the analysis with primary macrophages was also at 12 hours post-infection, while the analysis with THP-1 macrophages was at 16 hours post-infection.

To determine whether PBMC-derived M1 and M2 macrophages were susceptible to killing by VSV, we measured the viability of cells following VSV infection with an MTT assay. This assay tests for metabolic activity by measuring the reduction of a yellow tetrazolium dye to a purple formazan salt. Cells were infected with rwt or rM51R-M viruses at MOIs of 1 or 10 pfu/cell and viability was determined at 12- and 24-hours post-infection. The results in FIG 9 are expressed relative to the viability of mock-infected cells. PBMC-derived M2 macrophages demonstrated greater sensitivity to both rwt and rM51R-M-induced cell death as compared to M1 macrophages, with rwt virus exerting a greater effect on cell

killing than rM51R-M virus. The rwt virus reduced the viability of M2 macrophages by close to 60% at 24 hours post-infection at an MOI of 10 pfu/cell, while the reduction in viability at this time and MOI was only 17% for rM51R-M virus. In contrast, PBMC-derived M1 macrophages remained relatively resistant to killing by both viruses. Again, these data are in line with previous results obtained in THP-1-derived M1 and M2 macrophages (64).

Podosomes are Found at Different Locations within M1- and M2 PBMC-derived Macrophages

Next, we examined the podosomes of primary macrophages based on the presence of F-actin puncta. Macrophage podosomes include a precursor population of high density at the periphery and leading edge of motile cells and a successor population composed of less dense and more centrally located structures (32). Successor podosomes are derived from precursors before disassembling as part of podosome turnover (22). Based on F-actin staining and an accounting of punctate structures, PBMC-derived M1 macrophages had some amorphous F-actin staining that made podosome visualization more difficult they were more centrally located around the nucleus when seen [Note that nuclei are not depicted in the images for better resolution of F-actin puncta.] (FIG 10). In contrast, PBMC-derived M2 macrophages tended to have more densely staining F-actin puncta, usually away from the nucleus, and especially along the leading edge of the cells. These podosome localization patterns were not affected by infection with VSV, by either strain or at either MOI (FIG 10).

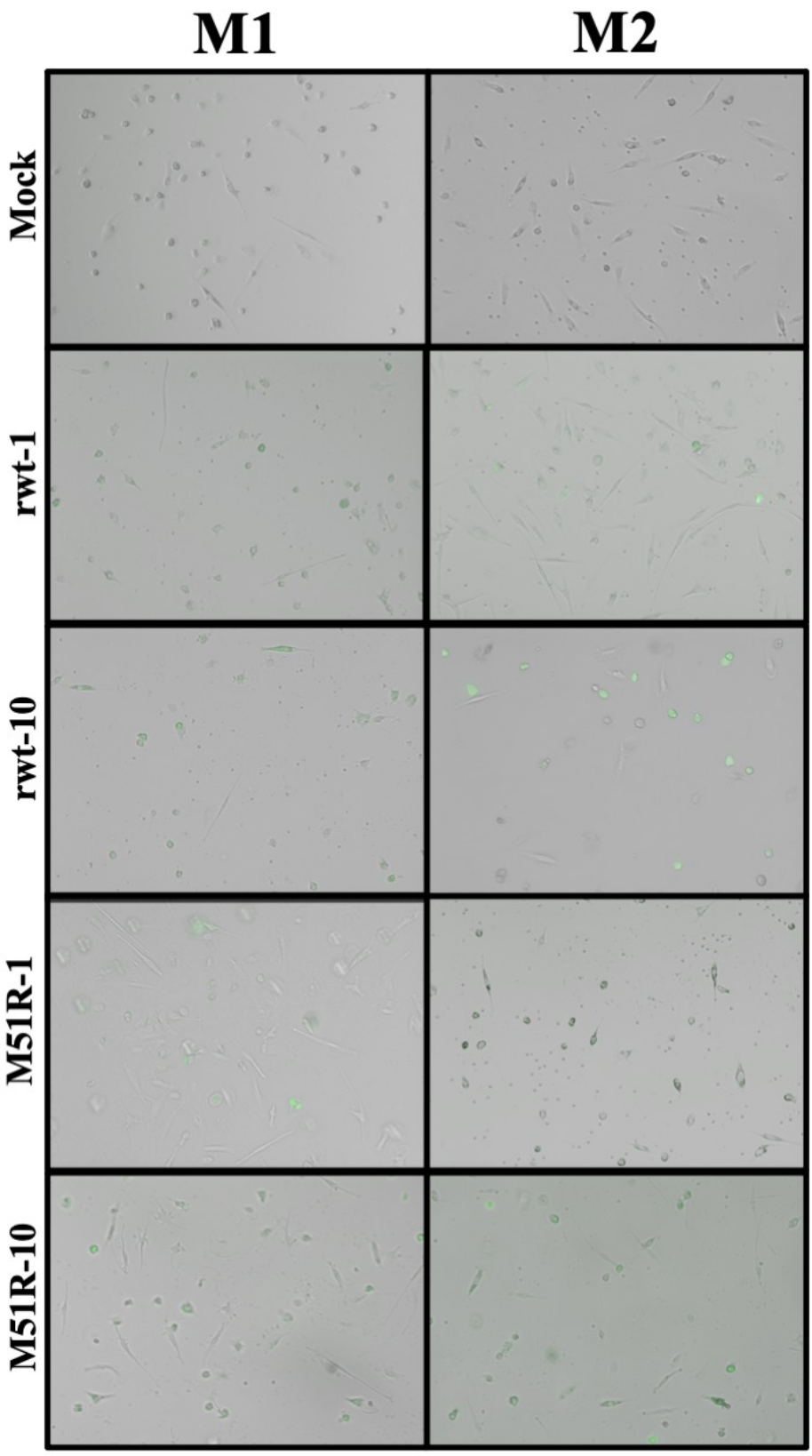

FIG 7 Representative Images of Viral Replication in M1 and M2 PBMC-derived Macrophages. PBMC-derived M1 and M2 macrophages were infected with or without (mock) rwt-GFP or rM51R-GFP virus at an MOI of 1 or 10 pfu/cell for 12 hours. Representative composite images of live cells by phase contrast and fluorescent microscopy are shown.

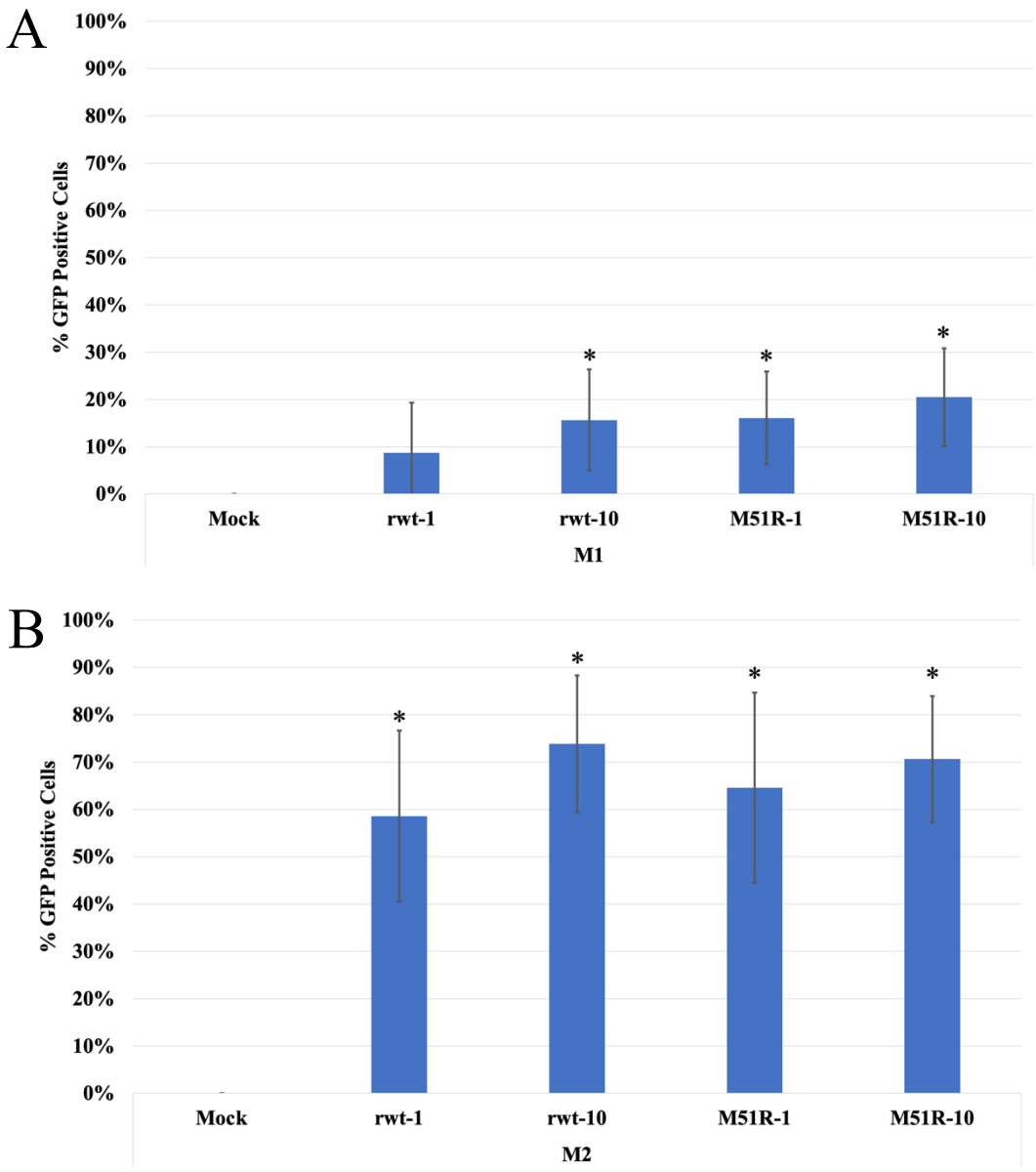

FIG 8 Differences in VSV Replication in M1 and M2 PBMC-derived Macrophages. PBMC-derived M1 (A) and M2 (B) macrophages were infected with or without (mock) rwt-GFP or rM51R-GFP virus at an MOI of 1 or 10 pfu/cell. Live cells were imaged at 12 hours post-infection by phase contrast and fluorescent microscopy. Ten, random images were used to determine the percentage of GFP-positive cells. Results are the average and standard deviation of three, independent experiments. Statistical analyses were conducted using a Student's t-test with significance determined at $p < 0.05$. * represents statistical differences between VSV-infected and mock-infected cells.

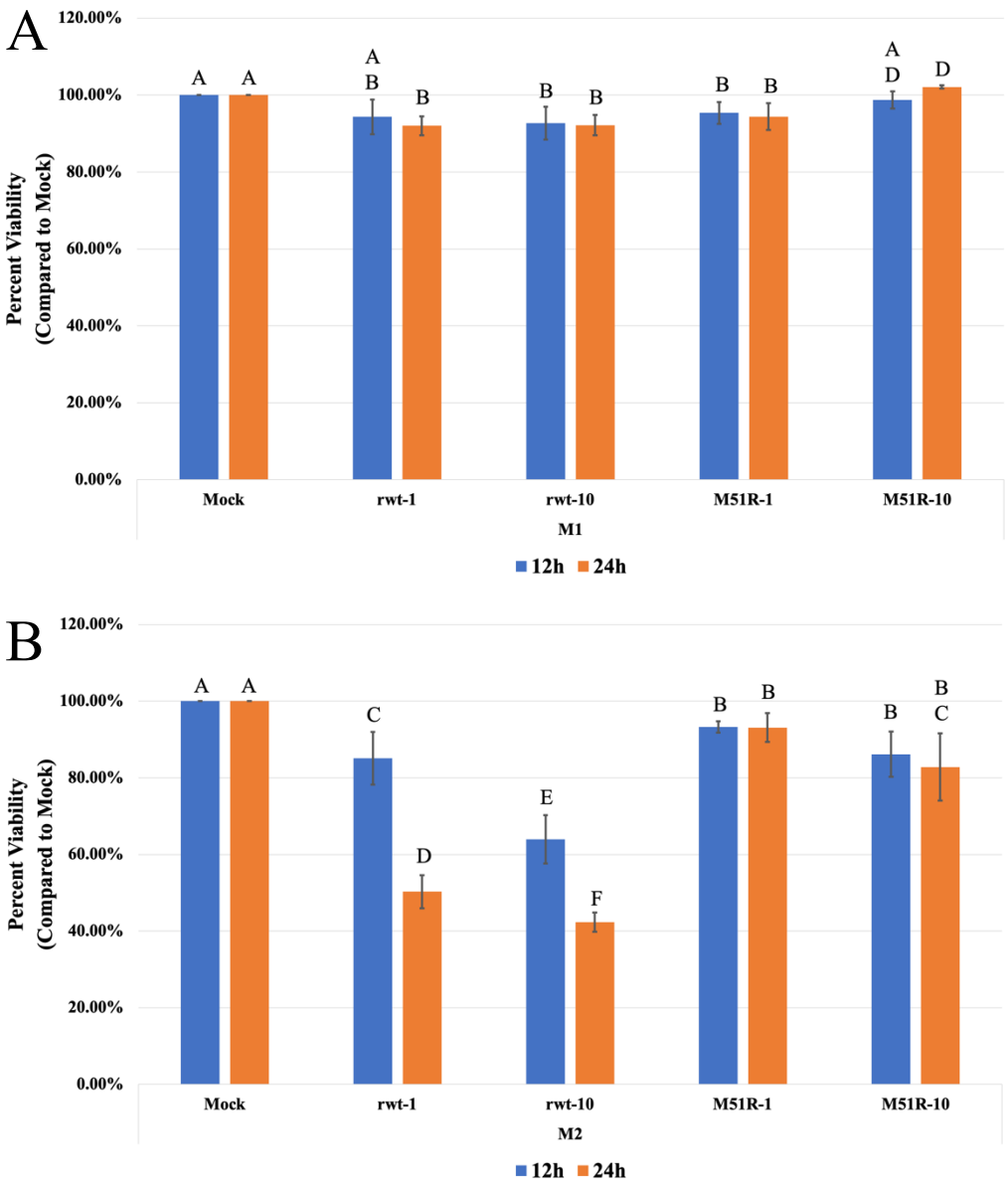

FIG 9 Differences in Viability in M1 and M2 PBMC-derived Macrophages With or Without VSV Infection. PBMC-derived M1 (A) and M2 (B) macrophages were infected with or without (mock) rwt or rM51R-M virus at an MOI of 1 or 10 pfu/cell for 12 or 24 hours before conducting an MTT assay to determine cell viability. Results are the average and standard deviation of triplicate measurements from three, independent experiments normalized to mock conditions at each timepoint. Statistical analyses were conducted using a Student's t-test with significance determined at $p < 0.05$. Statistical differences between conditions and timepoints are noted with differing letters.

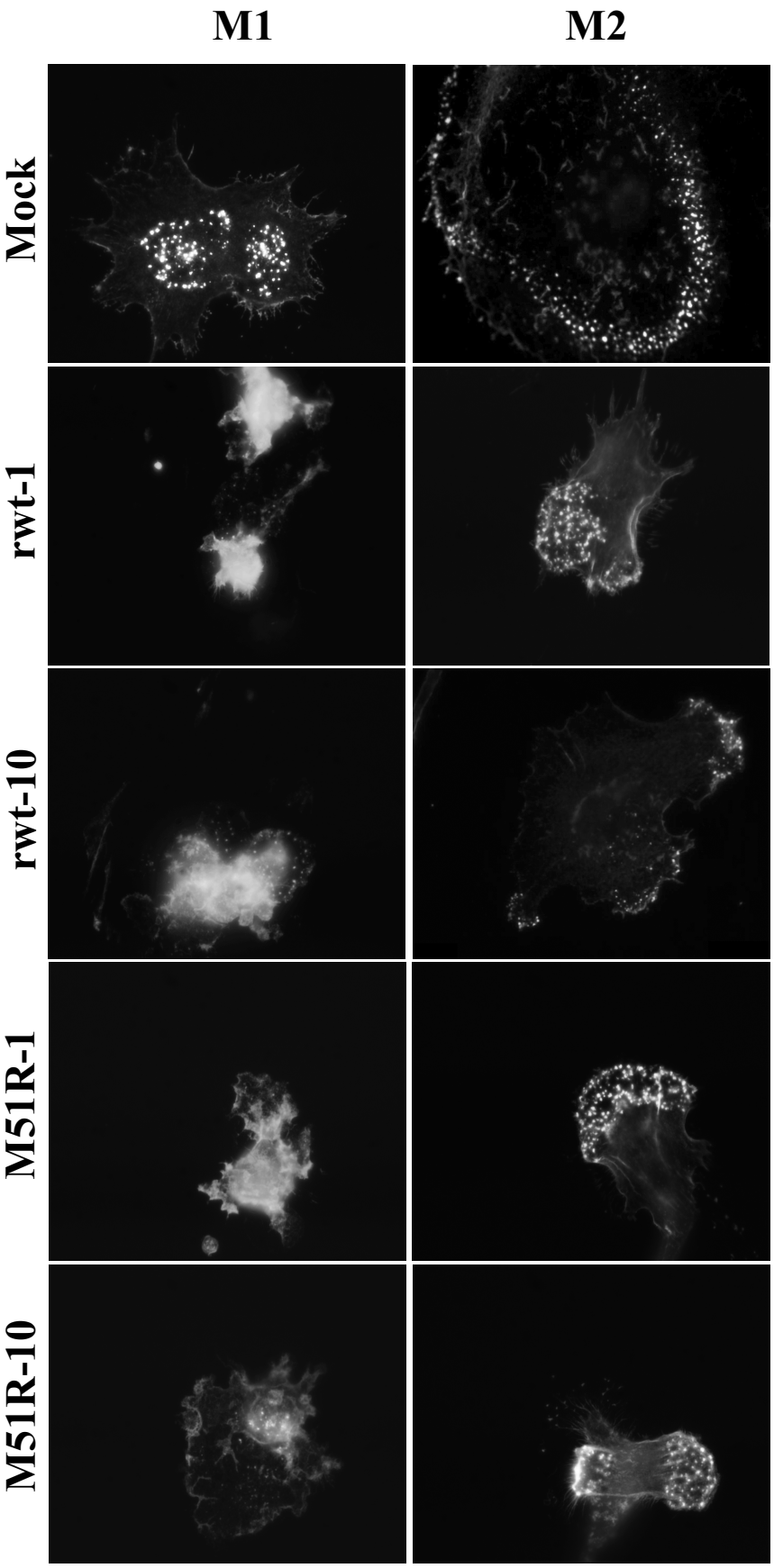

FIG 10 Representative Images of Podosomes in PBMC-derived M1 and M2 Macrophages. PBMC-derived M1 and M2 macrophages were infected with or without (mock) rwt-GFP or rM51R-GFP virus at an MOI of 1 or 10 pfu/cell for 12 hours. Cells were fixed and stained with Texas Red-X phalloidin to show F-actin-rich puncta indicative of podosomes.

M2 PBMC-derived Macrophages Podosome Multiplicity Exceeds that of M1 Macrophages and is Sensitive to VSV

In addition to their locations, podosome multiplicity was also determined in PBMC-derived M1 and M2 macrophages. Based on podosome counts in THP-1 macrophages, it was hypothesized that PBMC-derived macrophage podosome numbers would be higher in M2 macrophages (FIG 2). These results were confirmed (FIG 11). Indeed, M2 macrophages had 1.7-fold more podosomes/cell (~163/cell) than M1 macrophages (~95/cell). Despite there being a wide range in the number of podosomes/cell, there were no apparent outliers and the median of the data fell within one standard deviation of the mean. Interestingly, primary macrophages formed twice as many podosomes/cell than THP-1 macrophages in both macrophage subtypes (compare FIGs 2 and 13).

To determine the effects of VSV on the PBMC-derived macrophage podosomes, the cells were infected with rwt or rM51R-M virus at a MOI of 1 or 10 pfu/cell for 12 hours before staining for F-actin-rich puncta. It was again hypothesized, based on the published data in THP-1 cells, that primary M1 macrophage podosomes would remain the same after infection with both viruses while M2 macrophage podosomes would be reduced after infection with rwt virus, but not rM51R-M virus (FIG 2). Much of this was again the case. A skewedness test showed there were no significant differences between the mean and median across a wide range of podosome counts, and the average number of M1 macrophage podosome per cell were not significantly affected post-infection with rwt or rM51R-M virus at either MOI. In contrast, M2 macrophages infected with rwt did have significantly fewer podosomes than mock infected M2 macrophages, but infection with rM51R-M virus also

reduced the number of podosomes per cell. There was also a significant dose-dependent difference in the number of podosomes after infection with rM51R-M virus. This differed from the THP-1 model where M2 macrophage podosome multiplicity was reduced by this mutant strain of VSV, but not to statistically significant levels.

Taken together, primary M2 macrophages isolated from PBMCs have more podosomes than their M1 counterparts and they may be of the precursor variety based on

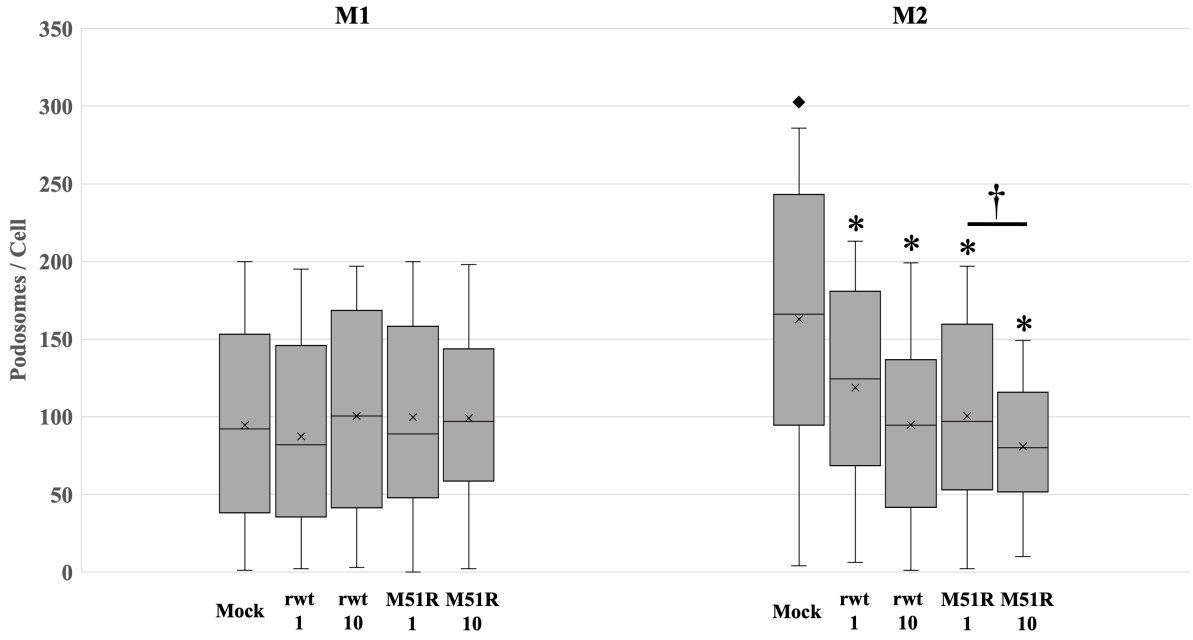

FIG 11 Differences in Podosome Multiplicity in M1 and M2 PBMC-derived Macrophages With or Without VSV Infection. PBMC-derived M1 and M2 macrophages were fixed and stained with Texas Red-X phalloidin to count F-actin-rich puncta indicative of podosomes. Results are derived from podosome counts in 20 cells from each macrophage subtype among three, independent experiments; *i.e.* 60 data points are shown for each macrophage subtype in the graph along with mean represented by "X" and median represented by a horizontal line. Statistical analyses were conducted using a one-way ANOVA with post-hoc Tukey HSD test. ⬩ represents statistical differences between M1 and M2 mock. * represents statistical differences between mock and viral infections. † represents statistical differences between the same virus at different MOIs.

their more peripheral location. However, these same cells are more susceptible to VSV infection and suffer more extensively from VSV's cytopathic effects (especially to rwt virus). Nevertheless, both viruses reduce podosome multiplicity in M2 macrophage, all the way to M1 levels, perhaps by different mechanisms.

Gene Expression Profiles Differ Between M1 and M2 PBMC-derived Macrophages

As with the THP-1 model system, we next tested whether the observed effects of rwt and rM51R-M virus seen in primary macrophages could be better understood mechanistically through a study of gene expression profiles. The results of this assay are shown in TABLE 4. First, all the ΔC_t values indicated upregulated transcript levels relative to the housekeeping gene GAPDH, though these differences were not statistically evaluated. Second, the $\Delta\Delta C_t$ analysis of the transcript ratio between PBMC-derived M2 to M1 macrophages set as a function of GAPDH showed a significant increase in 10 of the 13 transcripts assayed.

With regards to the M1 (MHC-II, STAT-1) and M2 (ARG-1, STAT-6) polarization transcripts analyzed, there was always higher levels of STAT-1, ARG-1, and STAT-6 in the M2 macrophages, with only MHC-II being unchanged between the macrophage subtypes. Given the immunoblotting results for p-STAT1 in FIG 6, it is clear that transcriptional profiling does not always equate to the protein levels of these polarization markers and certainly not their activation state, which cannot be assayed by this technique. Checking on the protein levels of each of these tested markers would be a reasonable step forward in checking the ultimate polarization status of these macrophage populations.

The transcripts for the actin regulatory protein Hck, as well as for all three of the actin nucleation proteins (Arp 2/3, cortactin, N-WASp), both podosome maturation/stabilization

proteins (dynamin 2, LSP-1), and the actin depolymerization protein cofilin were found in significantly higher levels in M2 macrophages compared to their M1 counterparts. There were no significant differences in the transcript levels for the podosome scaffolding protein Tks5 or for MMP-14. Both were readily increased under both polarization schemes, particularly Tks5.

Function	Gene	M1	M2	Ratio (M2/M1)
Actin Polymerization Promotion	**HCK**	21.12	50.79	2.40*
Actin Nucleation	**ARP 2/3**	109.74	304.18	2.77*
	Cortactin	63.33	157.96	2.49*
	N-WASP	18.23	65.00	3.57*
Podosome Structure	**Tks5**	533.08	719.23	1.35
Degradation	**MMP-14**	77.95	62.22	0.80
Podosome Stabilization	**Dyn 2**	38.73	229.33	5.92*
	LSP-1	116.93	617.46	5.28*
Actin Depolymerization	**Cofilin**	69.39	185.03	2.67*
M1 Marker	**MHC-II**	9.67	20.77	2.15
	STAT-1	55.43	110.85	2.00*
M2 Marker	**ARG-1**	16.87	93.00	5.51*
	STAT-6	28.55	67.38	2.36*

TABLE 4 Differences in Selected Podosome- and Polarization-associated Transcripts in M1 and M2 PBMC-derived Macrophages. PBMC-derived M1 and M2 macrophages were processed for qRT-PCR as described in TABLE 6. The ΔC_t values of each gene of interest are shown for M1 and M2 macrophages relative to GAPDH. The ratio is a $\Delta\Delta C_t$ measurement whereby the ΔC_t of the M2 macrophage transcript of interest was divided by the ΔC_t of the same transcript in M1 macrophages. Results are the average of three, independent experiments. Statistical analyses were conducted using a Student's t-test with significance determined at $p < 0.05$. * represents statistical differences between M1 and M2 macrophages. Heat map colors were generated using the logarithm of the M2/M1 ratio.

VSV Exerts Differential Effects on Podosome- and Polarization-associated Gene Expression in M1 and M2 PBMC-derived Macrophages

After determining baseline transcript levels for the selected podosome and

polarization markers in PBMC-derived M1 and M2 macrophages, both subtypes were subjected to infection with rwt or rM51R-M virus at an MOI of 1 or 10 pfu/cell for 12 hours before processing the cells for qRT-PCR analysis. Results for PBMC-derived M1 and M2 macrophages are shown in TABLE 5. Successful infection by VSV is indicated by the significant upregulation of the N protein transcript in both macrophage subtypes in response to both viral strains and at both MOIs. Despite the greater resistance of PBMC-derived M1 macrophages to viral infection (TABLE 3A), the $\Delta\Delta C_t$ values for VSV N were higher in M1 macrophages (8.87-fold with rM51R-M virus at an MOI of 10 pfu/cell) than M2 macrophages (4.25-fold with rwt virus at an MOI of 10 pfu/cell), though these differences were not analyzed statistically.

The $\Delta\Delta C_t$ analysis of polarization markers in infected M1 and M2 macrophages showed some striking, but not altogether predictable, changes in response to VSV infection. For example, expression of the M1 marker MHC-II was always higher following VSV infection in M1 macrophages suggesting that the virus has little impact on M1 polarization (TABLE 5A). However, the other M1 marker STAT-1 was always reduced following VSV infection, and this was true in both M1 and M2 macrophages (TABLE 5). Even more striking was the upregulation of the M2 marker ARG-1 in VSV-infected M1 macrophages (TABLE 5A). This might imply that the virus can induce a polarization shift from M1-to-M2 macrophages, or at the least create some intermediate phenotype. On the flip side, the M2 markers ARG-1 and STAT-6 were often down-regulated in M2 macrophages following VSV infection, arguing for M2-to-M1 repolarization (TABLE 5B). Analysis of these polarization markers at the protein level, as suggested earlier, is clearly warranted.

Lastly, we looked at podosome marker transcript levels in primary M1 and M2 macrophages in response to VSV infection. In M1 macrophages there was an upregulation of Arp 2/3 and dynamin 2 under all conditions and to Hck and N-WASp with both viruses at an MOI of 10 pfu/cell (TABLE 5A). However, downregulation was seen for Tks5 (all conditions), and for cortactin, LSP-1, and cofilin (both viruses). In M2 macrophages, dynamin 2 was also upregulated (both viruses) and Tks5, LSP-1, and cofilin were also downregulated (both viruses); however, the other markers showed different results from M1 macrophages with Arp 2/3 levels being unchanged, and both Hck and N-WASp being downregulated (both viruses) (TABLE 5B). Recalling the near universal upregulation of podosome transcripts in M2 THP-1 macrophages (TABLE 3B), the results seen here again argue for distinct model system responses.

A

Function	Gene	rwt-1	rwt-10	M51R-1	M51R-10
Viral Load	**VSV N**	2.12*	3.82*	3.22*	8.87*
Actin Polymerization Promotion	**HCK**	1.15	1.25*	1.11	2.13*
Actin Nucleation	**ARP 2/3**	2.98*	3.08*	2.68*	7.68*
	Cortactin	2.00	0.19*	0.36*	2.03
	N-WASP	0.38*	5.01*	0.63*	6.50*
Podosome Structure	**Tks5**	0.76*	0.13*	0.11*	0.30*
Degradation	**MMP-14**	1.31	0.79	0.73	0.61*
Podosome Stabilization	**Dyn 2**	5.98*	6.04*	4.00*	14.04*
	LSP-1	0.47*	0.25*	0.07*	0.93
Actin Depolymerization	**Cofilin**	0.33*	0.57*	0.43*	2.07
M1 Marker	**MHC-II**	2.73*	3.46*	3.16*	7.42*
	STAT-1	0.06*	0.08*	0.06*	0.09*
M2 Marker	**ARG-1**	2.49*	3.77*	2.62*	3.58*
	STAT-6	1.05	1.06	0.34*	1.53

B

Function	Gene	rwt-1	rwt-10	M51R-1	M51R-10
Viral Load	**VSV N**	1.63*	4.25*	1.08*	1.90*
Actin Polymerization Promotion	**HCK**	0.75*	1.29	0.38*	1.15
Actin Nucleation	**ARP 2/3**	1.52	1.88	0.90	1.56
	Cortactin	4.47*	0.09*	0.34*	0.21*
	N-WASP	0.12*	0.85	0.36*	0.46*
Podosome Structure	**Tks5**	0.71*	0.05*	0.16*	0.17*
Degradation	**MMP-14**	3.38*	1.27	0.99	1.88
Podosome Stabilization	**Dyn 2**	1.04	2.47*	1.03	1.91*
	LSP-1	0.77	0.04*	0.09*	0.21*
Actin Depolymerization	**Cofilin**	0.17*	0.15*	0.45*	0.65*
M1 Marker	**MHC-II**	1.37	1.85	2.04	2.46
	STAT-1	0.04*	0.05*	0.06*	0.08*
M2 Marker	**ARG-1**	0.46*	0.67*	0.93	0.90
	STAT-6	1.04	0.41*	0.70*	0.42 *

TABLE 5 Differences in Selected Podosome- and Polarization-associated Transcripts in M1 and M2 PBMC-derived Macrophages With or Without VSV Infection. PBMC-derived M1 (A) and M2 (B) macrophages were infected with or without (mock) rwt or rM51R-M virus for 12 hours at an MOI of 1 or 10 pfu/cell. Cells were processed for qRT-PCR analysis as described in TABLE 6. Displayed are the $\Delta\Delta C_t$ analyses comparing each of the VSV-infected conditions to the mock condition for each gene of interest. Results are the average of three, independent experiments. Statistical analyses were conducted using a Student's t-test with significance determined at $p < 0.05$. * represents statistical differences between VSV-infected and mock-infected cells. Heat map colors were generated using the logarithm of the VSV-infected/mock-infected ratio.

CHAPTER 4: DISCUSSION

It has been proposed that the ECM-remodeling properties of M2 macrophage podosomes supports cancer cell growth, angiogenesis, and metastasis. Since our lab has evidence that oncolytic VSV destroys M2 macrophages or alters them to a more tumor-fighting M1-like state, it is possible that podosome development might be compromised in this cell type following VSV infection as well (64). We set out to study the podosomes of THP1 and PBMC-derived M1 and M2 macrophages following infection with two different VSV strains (rwt, rM51R-M) in order to better appreciate the effects of this new form of cancer therapy within the tumor microenvironment. Two goals were undertaken: (i) establish baseline measurements of podosome numbers, podosome-associated ECM degradation, and podosome marker expression in M1 versus M2 macrophages, and (ii) determine the impact of VSV infection on these podosome-associated properties. Our findings can be summarized with the following conclusions. (i) Podosomes are common to both M1 and M2 macrophages whether they are from the THP-1 cell line or from primary cells. (ii) Podosome numbers are higher in M2 versus M1 macrophages and they may exhibit a polarized localization towards the leading edge of motile cells as so-called precursor podosomes. However, (iii) podosome-associated gelatin degradation, measured as a surrogate for ECM remodeling, occurs at a faster rate in M1 THP-1 macrophages, though M2 macrophages catch up by 24 hours. [This property was not tested in primary cells.] (iv) Both VSV strains, and particularly rwt virus, selectively reduce podosome numbers exclusively in M2 macrophages, whereas both VSV strains, and particularly rM51R-M virus, selectively reduce matrix-degrading podosome activity exclusively in M1 macrophages. And, (v) measurement of podosome transcripts in

both macrophage models and macrophage subtypes in response to both VSV strains might suggest an intermediate macrophage phenotype following VSV infection.

Mechanisms for Increased Podosome Multiplicity in M2 THP-1 Macrophages

Podosome multiplicity data from the THP-1 cell line showed that M2 macrophages had significantly more podosomes than M1 macrophages under normal physiological conditions (FIG 2). We tested whether podosome marker transcript levels might be predictive of those distinct phenotypes.

The most significant increases in mRNA in M2 THP-1 macrophages were for N-WASp, dynamin 2, and cofilin (TABLE 6). N-WASp has a role in actin nucleation by the Arp 2/3 complex and thereby an important roles in the synthesis of new actin microfilaments, and thus new podosomes (42, 108). Arp 2/3 transcripts were, however, unchanged in this study. Dynamin 2 is a GTP-binding protein associated with microtubules and helps bend the plasma membrane outward as the podosome extends into the ECM (109). Perhaps this explains the additional numbers of podosomes in M2 macrophages as well. Finally, cofilin functions to sever actin microfilaments, thus causing the retraction of podosomes back into the cell (105). The increase in cofilin may suggest a higher turnover rate and therefore more dynamic M2 macrophage podosomes. This dynamic podosome arrangement does not argue for or against the increased podosome numbers in M2 macrophages, but may relate more to their rapid movement through tissues during the invasion process.

The most significant increases in mRNA in M1 THP-1 macrophages were MMP-14 (discussed above) and cortactin (TABLE 6). Like N-WASp, cortactin is an actin nucleation protein. Here, the high transcript levels might be predictive of the increased rate of ECM

degradation seen in this macrophage subtype. Or perhaps the reduced levels of dynamin 2 in M1 macrophages (relative to M2 macrophages), which is also known to help stabilize podosomes, might explain the previously hypothesized high podosome turnover in M1 macrophages where more dynamic podosomes might sample more of the gelatin matrix.

We must also acknowledge that transcript levels cannot report on the many post-transcriptional regulatory mechanisms governing podosome development. Cortactin, for example, is regulated by missing in metastasis (MIM) protein, extracellular signal-regulated kinases (ERK) 1/2, and $p47^{phox}$ (108, 110, 111). Phosphorylation by FAK is a primary regulator of N-WASp (112). And cofilin is regulated by slingshot protein phosphatases (SSHs) that activate the protein and LIM kinase-dependent phosphorylation that inactivates it. Levels of phosphorylated cortactin, N-WASp, and cofilin were not determined in this study.

Mechanisms for Increased Podosome Activity in M1 THP-1 Macrophages

Podosome multiplicity data from the THP-1 cell line showed that M2 macrophages had significantly more podosomes than M1 macrophages under normal physiological conditions (FIG 2). We naturally presumed that having more podosomes in M2 THP-1 macrophages would translate to greater ECM degradation ability among this subtype. However, the *in situ* zymography assay used to monitor podosome activity showed that M1 macrophages degrade significantly greater amounts of gelatin at the onset of cell seeding (FIG 4). There are several potential reasons for these observations: (i) M1 macrophage podosomes could be producing higher levels of MMPs or other ECM-remodeling proteinases, (ii) M1 macrophage podosomes could have a higher rate of turnover that enables

them to sample more gelatin over time, (iii) M1 macrophage podosomes may have higher amounts of integrins that enable more rapid adhesion to and/or migration upon the provided substratum, and/or (iv) M1 macrophage podosomes may be better at degrading gelatin under the 2D conditions of the *in situ* zymography assay used in this study.

In an analysis of podosome transcript levels by qRT-PCR, we showed that M1 THP-1 macrophages do have significantly higher levels of the transmembrane proteinase MMP-14 than do M2 macrophages. In 2D podosome degradation and migration studies, MMP-14 has been shown as the predominant proteinase present within macrophage podosomes (113). MMP-14 is also largely regulated at the transcriptional level, thus the amount of MMP-14 mRNA should be in direct correlation with MMP-14 protein levels (114). There are also other proteinases that can be secreted by macrophages, such as MMP-2 and MMP-9, cathepsin S, cathepsin B, and cathepsin L, and the urokinase plasminogen activator surface receptor (uPAR) (60, 113). These were not analyzed in this study, but higher levels of any of these MMPs could partially explain the gelatin degradation differences between M1 and M2 THP-1 macrophages that were observed.

Turnover is a term used to describe a stage of podosome development; *i.e.* the point at which the cap proteins begin to disassemble and the actin microfilaments are severed, thus leading to podosome instability. Podosome lifetime in macrophages ranges from 0.5 to 14 minutes with a median of 2.5 minutes (15, 61). Supervillin is known to mediate cap protein disassembly and the retraction of podosomes back into the cell via myosin-IIA cables, but the entire turnover process in macrophages is not well known and is a current subject of investigation by various research groups (32, 33). Because of the lack of evidence behind

supervillin regulation of macrophage podosome turnover, this transcript was not investigated in this study.

Transmembrane integrin receptors enable the podosome (or the cell in general) to adhere to the ECM (18). Proteomic analysis shows that β2 integrin is the primary adhesion receptor in macrophage podosomes. β1 integrin can be found within the podosome core, while β2 and β3 integrins can be found within the adhesion ring (115). A cell with a greater number of integrin receptors embedded into the plasma membrane might logically allow for a higher rate of degradation due to the increased ability of cells to adhere to the ECM. Integrin composition or quantity were not measured as a part of this study, but it is worth mentioning that the podosome multiplicity assay was conducted with cells that had been polarized and fixed on glass coverslips for 72 hours, while the gelatin degradation assay started with polarization of cells on treated cell culture dishes before being lifted with Accutase and transplanted onto gelatin for up to 24 hours. Although both methods are commonly used to monitor podosome development, only the latter technique addresses the early events in this process. It is also an open question as to what is happening to the podosomes of the cells and their membrane-associated marker proteins (*e.g.* MMP14, integrins, etc.) after the cells are lifted, which also was not addressed in this study. Not presented in this study was an early attempt to fully polarize THP-1 macrophages in the presence of GM-6001, a broad-spectrum MMP inhibitor (data not presented). The goal was to polarize the cells, then wash away the drug, so that the cells could be allowed to start degrading gelatin at a desired point in the assay (*i.e.* after VSV infection), without going through the passaging process. Although the cells were drugged with varying GM-6001 concentrations, it was not able to stop gelatin degradation for the full polarization period.

This may mean the cells are able to produce higher levels of MMPs than GM-6001 can bind to and inhibit the function of, or that there may be additional degradation pathways the cells are able to employ for this purpose (116).

Finally, *in situ* zymography is a 2D assay specifically designed to look at the differences in podosome activity on the ventral surface of cells where they are found *in vitro*. Previous studies from the Maridonneau-Parini lab specifically looked at a different non-polarized model of human-derived macrophages for podosome development, ECM degradation, and motility in both 2D and 3D (24). In a 2D gelatin environment, macrophages were shown to form greater numbers of podosomes with longer lifespans than those cultured in a 3D environment. In addition, previous studies have shown that M1 macrophages are capable of only an amoeboid-type movement, meaning that the cells extend a leading edge into substrate and use actin-myosin-based contractility to squiggle the back end of the cell forward through gaps in the ECM (117). Amoeboid movement happens very quickly with relatively low amounts of adhesion and proteolysis. M2 macrophages, however, are capable of both amoeboid and mesenchymal movement, the latter being cells that degrade the ECM as they push forward. Such mesenchymal movement happens slowly with strong adhesion, especially along the leading edge of the cell (118). Previous studies have shown that integrin-based cell-matrix adhesion is not required for M1 macrophage amoeboid migration; however, it is requisite for mesenchymal migration of M2 macrophages (117). Since integrin adherence is not required in M1 macrophage degradation and motility, this may explain why M1 macrophages are able to degrade ECM at a higher initial rate than M2 macrophages, which require adherence to the substratum.

Mechanisms for Decreasing THP-1 Macrophage Podosome Development Following VSV Infection

M1 THP-1 macrophages infected with rwt virus reduced podosome numbers at an MOI of 1 pfu/cell, and initially reduced podosome-associated gelatin degradation at 6 hours post-infection at both MOIs (FIGs 2 and 5). Gelatin degradation, however, did recover by the 12- and 24-hour timepoints. In contrast, M1 macrophages infected with rM51R-M virus did not sustain changes in podosome multiplicity but had a significant decrease in gelatin degradation at 6, 12, and 24 hours. One mechanism for explaining these disparate results is that anti-viral factors, such as those within the type I IFN response, are somehow inhibiting matrix degradation. This is consistent with previous studies that found transcriptional suppression of MMP-9 after treatment with IFN-γ and IFN-β via a STAT-1α dependent mechanism (119).

While M2 macrophages are more susceptible to infection with rwt virus and their podosome numbers are also reduced by this viral strain, there was no effect on ECM degradation (120). The only clear transcript in the gene expression assay that could explain this is the trending increase in MMP-14. Perhaps other MMPs not studied in this thesis, most notably MMP-2 and MMP-9, impact ECM degradation in infected M2 macrophages as well (121).

Nuances of Common Macrophage Model Systems

In order to determine how different populations of macrophages respond to a variety of stimuli, one model that is widely employed is the THP-1 cell line. THP-1 cells were derived from a 1-year-old human male with acute monocytic leukemia (122). The cells are

easily cultured and have been in continuous ubiquitous use in biomedical research since their discovery in the 1980s, but how well do they simulate *in vivo* conditions? THP-1 monocytes are distinct in that not only are they an immune cell, but they are also a cancer cell. A hallmark of leukemic cancers is the rapid generation of non-maturing blast cells. Therefore, in the absence of treatment by any reagent, THP-1 monocytes do not differentiate, and the agent used to direct macrophage differentiation, the phorbol ester PMA, is not naturally found in the human body.

It is not uncommon for researchers to confirm results with cell lines to results with primary cells, either from research animals or human volunteers. Macrophages can be obtained through various harvesting methods including collection from the peritoneum following macrophage induction, the bone marrow, or the peripheral blood. The collection of peripheral blood and isolation of mononuclear cells is one of the easier ways to obtain primary monocytes (123-125). This mixture of peripheral blood mononuclear cells (PBMC) includes not only monocytes, but also dendritic cells, T cells, B cells, and natural killer cells. Only the monocytes adhere to the bottom of the dish and these isolated monocytes can now be differentiated and/or polarized to the different populations of macrophages studied here.

PBMC-derived Macrophages Exhibit Similar THP-1 Derived Macrophage Behaviors

While the Seals and Ahmed labs have previously published on the impact of VSV on THP-1 M1 and M2 macrophages, virus replication and virus-induced cytopathic effects in PBMC-derived macrophage populations had not been investigated until this study (64). To more closely evaluate the ability of VSV to replicate in and kill M1 and M2 macrophages derived from THP-1 cells versus PBMCs, a comparison of the results in these two model

systems are shown in Table 1. Our results revealed similarities. For example, M1 macrophages are significantly more resistant to VSV infection than M2 macrophages, and this is true in both model systems, though PBMC-derived macrophages are generally more sensitive to viral replication than model THP-1 macrophages. Viability data in both macrophage models are consistent with the replicative ability of the virus. As replication of the virus increases in macrophages, its cytopathicity towards macrophages increases as well. Finally, podosome multiplicity is higher in M2 macrophages than M1 macrophages and both rwt and rM51R-M virus can reduce M2 macrophage podosome numbers to M1 macrophage levels in both model systems.

Assay	THP-1 Model		PBMC Model	
	M1	**M2**	**M1**	**M2**
Sensitivity to VSV Replication	Extremely Resistant	Sensitive	Resistant	Sensitive
VSV Cytopathicity	Extremely Low	rwt – High rM51R-M – Mod	Extremely Low	rwt – High rM51R-M – Mod
Podosome Multiplicity	~ 51 / cell	~ 92 / cell	~ 95 / cell	~ 163 / cell
VSV Effect on Podosome Numbers	NC	rwt - ↓ rM51R-M - NC	NC	↓
Podosome Activity	High	Moderate	N/A	N/A
VSV Effect on Gelatin Degradation	↓	NC	N/A	N/A

Table 6 A Data Comparison of THP-1 and Primary Macrophage Models in Response to VSV Infection. An overall comparison of THP-1 and PBMC-derived macrophages as it relates to their M1 and M2 polarization status, podosome competency, and effect of VSV infection thereof. Mod, Moderate; NC, No Change.

Mechanisms for Decreasing Primary Macrophage Podosome Development Following VSV Infection

We found that in support of the podosome multiplicity data from PBMCs that M2 macrophages are significantly upregulated in all podosome transcripts analyzed with the exception of Tks5 and MMP-14 (TABLE 4). This would indicate the ability of M2 macrophages to better assemble and stabilize their podosomes than M1 macrophages. Although M1 macrophage podosome multiplicity wasn't affected by VSV infection, there were still wide changes in podosome markers. However, these are not likely to be key mediators of the number of podosomes in a cell, and/or there is proteomic level of podosome regulation that supersedes the transcriptional processes that may be involved. Furthermore, the inability to gain additional mechanistic information may have been constricted by the number of podosome transcripts that were analyzed as well as additional factors in key pathways (such as the type IFN pathway) that may be responsible for some of the functional differences we have observed.

Possible Benefits of rM51R-M Virus as an Anti-M2 Macrophage Therapeutic

The purpose of investigating outcomes using two VSV strains like rwt and rM51R-M was to investigate their effects on macrophage podosomes during infections that either are or are not immunogenic. The M-protein mutant virus is considered to be a safer therapeutic option than its wild-type counterpart because it induces an anti-viral response that allows the host to retain some control in attenuating viral replication (126). While it is true that wild-type field strains of VSV exert low pathogenicity in humans, it can still be neuropathogenic in mice and non-human primates (127-130). However, like any biological agent used as a

therapeutic in humans with potentially weakened and defective immune systems, it is important to engineer the therapeutic agent in a manner than reduces pathogenic effects in human hosts, similar to the mutation existing in rM51R-M virus.

There are a couple of potential drawbacks in using rM51R-M virus as an anti-cancer agent as it pertains to TAM populations. First, it is not as cytopathic as rwt virus and thereby may leave more M2 macrophages within the TME. Second, it showed some ability to reduce the ECM degradation capabilities of M1 THP-1 macrophages (FIG 5). If so, then M1 macrophages might be disabled in their ability to penetrate the TME to exert their anti-cancerous effects. However, there are many benefits to this kind of therapy as well. This includes: (i) its safety features based on stimulating anti-viral immunity, (ii) its ability to kill up to 20% of M2 macrophages (FIG 9), (iii) its ability to reduce podosome number in M2 macrophage populations thereby disarming these cells of their pro-cancerous invasive features (FIGs 2 and 13), and (iv) its ability to induce a possible phenotypic switch from M2-like macrophages to a more M1-like macrophage (64).

Elucidating Macrophage Phenotypes Post-infection with VSV

The M1/M2 paradigm was originally proposed in the early 2000's to relate to the well-known activation status of T-cells (Th1/Th2) (1). However, since the adoption of that nomenclature, it has been discovered that there are far more phenotypes than just M1 and M2, and that these phenotypes often fall somewhere on a spectrum between these two polarization extremes. Some researchers have adopted an M1-like and M2-like nomenclature when discussing macrophage phenotypes.

Previous studies in the Ahmed and Seals laboratories have suggested that rM51R-M virus induces a M2-to-M1 macrophage phenotypic switch as indicated by the increased phosphorylation of STAT1 in both the THP-1 and primary macrophage models (64). THP-1-derived M2 macrophages also have increased expression of the cell surface costimulatory molecule CD80 as well as increased secretion of TNF-α following infection with rM51R-M virus, all consistent with M1 repolarization (64, 100). However, the data presented here indicate that it may be too simplistic to conclude that rM51R-M virus repolarizes M2 to true M1 macrophages. Indeed, after analysis of both THP-1- and PBMC-derived macrophages, questions of polarization status remain because of the differences in, for example, ARG-1 expression, an M2 marker that was upregulated in M1 macrophages following infection with VSV. In addition, the aforementioned study also showed that THP-1 M2 macrophages that were infected with rM51R-M virus continued to express CD206 12-hours post-infection, as well as pSTAT-1. Such data implies that the same virus that repolarizes M2 macrophages to a more intermediate phenotype may also be repolarizing M1 macrophages to an intermediate phenotype as well.

CHAPTER 5: CONCLUSION

Oncolytic VSV Targets Macrophage Podosomes

VSV has been developed for well over two decades as an anti-cancer therapeutic because of its oncolytic capabilities. In addition, due to recent advances in genetic technologies and the ease of manipulating the VSV genome, genes for immunostimulatory molecules such as IFN-β, various interleukins, and dendritic cell activation factors (Flt3L) have been engineered into the viral genome (131). Furthermore, additional strategies include the induction of antigen-specific CD8+ T cell responses through the delivery of xenogeneic peptides like dopachrome tautomerause (DCT) or tumor-associated antigens like gp100 by VSV (95, 132, 133). However, development of VSV as an agent that impacts podosome development in macrophages is intriguing and warranted the research efforts presented in this study.

Even as podosomes may stimulate the metastatic cascade, therapeutics directly targeting macrophage podosome development are lacking. Currently there are two drugs targeting proteins of the related invadapodia of cancer cells. Denosumab targets RANKL and trastuzumab targets HER2, both of which are upregulated in highly invasive cancer cells that commonly develop podosome-like invadopodia (68). An additional therapeutic targets MMPs (ilomastat/GM-6001) and may thereby inhibit macrophage podosome activity as it relates to ECM degradation. However, these therapies do not necessarily address the contribution of macrophage podosomes during the cancer process. The results presented in this study consider how VSV as an oncolytic therapy may impact the functions of TAMs. Specifically, we showed that rwt virus inhibited M2 macrophage podosome development in

both the THP-1 and the PBMC model systems. rM51R-M virus was also successful at inhibiting podosome development in PBMC-derived macrophages. A new therapeutic regimen that combines the potential of VSV to not only target and kill cancer cells, but also repress the metastatic process through inhibition of macrophage podosome development, all while inducing anti-tumor immunity, would greatly assist cancer patients at potentially all stages of cancer progression.

Future Directions

This study has advanced our understanding of the THP-1 model system as it relates to podosome development and has introduced the PBMC-derived macrophage model for a similar purpose. The information gained from these model systems has helped in determining how oncolytic VSV strains modulate the development of M1 and M2 macrophage podosomes, including their role in degrading the ECM. While we have gained valuable insights from these studies, additional studies can be envisioned moving forward.

Gelatin Degradation for PBMC-derived Macrophages

One of the key experiments to complete in this study is to determine the ability of PBMC-derived macrophages to degrade the ECM. Results from this assay would allow us to compare the degradative abilities of PBMCs to that of THP-1-derived macrophages. Additional questions we could answer from this assay are: (1) what are the differences in the degradative abilities of PBMC-derived M1 and M2 macrophages and (2) how does VSV affect the development of PBMC-derived macrophage podosomes and their function? In the THP-1 model, we found that M2 macrophages have more podosomes than M1 macrophages,

but degradation of a gelatin matrix was significantly higher for M1 macrophages, at least initially after cell plating. At later timepoints, M2 macrophages regained the ability to degrade gelatin to similar levels as M1 macrophages. Perhaps the PBMC model could help determine the mechanisms behind this discrepancy. For example, we could measure levels of MMPs or other matrix-degrading proteases produced by each phenotype to test whether the initial decrease in degradation seen in M2 macrophages is due to lower levels of proteases at the podosome sites. Rates of adhesion and motility in cells could also be explored for both models to give possible insights into why M1 macrophages degrade significantly more than M2 macrophages at early timepoints.

Podosome Multiplicity After Lifting Cells

One key methodological difference between the podosome multiplicity analysis and the gelatin degradation analysis was the lifting and replating of pre-polarized cells onto the gelatin coverslips. Due to the lack of understanding of how podosomes develop when cells have been lifted and replated, it is difficult to make direct comparisons to conditions in which cells remain plated. By analyzing these experimental differences, we may gain additional insight and understanding as to why M1 macrophages degrade gelatin to higher levels at early time points as compared to M2 macrophages.

Precursor Versus Successor Podosomes

One observation we made in this study was the appearance of greater numbers of precursor podosomes than successor podosomes in PBMC-derived M2 macrophages. As a reminder, precursor podosomes display as denser podosomes around the leading edge of the

cell while successor podosomes have less density and are localized to the central body of the cell. Successor podosomes are considered end-stage podosomes that were once highly functional precursors on the leading edge of the cell but are undergoing disassembly and loss of function. It would be interesting to investigate the differences in the number of precursor and successor podosomes within M1 and M2 macrophages. This may answer the questions of why M1 macrophages may be initially better at adhering to gelatin to begin the degradation process and why there is greater ECM degradation over time in M2 macrophages as opposed to M1 macrophages.

3D Degradation and Mobility Assay

As previously mentioned, all measurements of gelatin degradation in this study were conducted using a 2D *in situ* zymography assay. While this assay represents an important tool to allow measurement of ECM degradation by macrophage podosomes, it does not give a completely accurate picture of what these cells may do in the 3D environment of the body. Previous studies have found a great number of differences between 2D and 3D assays for PBMC-derived M0 macrophages including a greater number of podosomes with longer lifespans in 2D cultures than in 3D cultures (24). Since the studies undertaken in the Seals and Ahmed labs focus on investigating the differences between M1 and M2 macrophages and the impact of VSV infection on both populations, it will be important to carry out assays in a 3D matrix, which more closely mimics the natural environment of these cell types. These studies could also give additional insight into why M1 THP-1 macrophages have higher degradative abilities at early times than M2 macrophages. Previous literature has shown that M1 macrophages are only capable of amoeboid movement and must “throw out” additional

proteases for ECM degradation in order to squeeze between thin openings while M2 macrophages utilize a more directed mesenchymal movement involving the focalized ECM degradation patterns consistent with podosomes (117). By carrying out studies in a 3D environment consisting of a block of fibrillar collagen, we can determine whether our observations are consistent with this finding.

3D Invasion and Co-Culture

In addition to the 3D assay mentioned above in which motility and ECM degradation by macrophages in a fibrillar collagen block would be determined, it is important to determine the invasive characteristics of these polarized macrophages. Future studies will also seek to experimentally measure the ability of macrophages to assist in the invasion of malignant cells. These studies will utilize an invasion assay in which fluorescently conjugated antibodies to macrophage markers will determine the degree of macrophage movement through the 3D collagen or Matrigel matrix, while fluorescently-tagged cancer cell lines will be utilized to measure the invasive capabilities of cancer cells in that environment. Increased invasion of specific macrophage subtypes into fibrillar collagen or the denser Matrigel matrix may reveal differences in invasive capabilities of one macrophage subtype over another and give insights into the impact of VSV on their invasion abilities. At the same time, using cancer cell types with different invasive capabilities may reveal additional details about the contributions of macrophage populations to the metastatic process. For example, if a specific macrophage population increases the invasive capabilities of a less invasive cancer cell line, it serves to promote the metastatic process. On the other

hand, decreasing the invasion of a highly invasive cancer cell indicates that the macrophage phenotype may be anti-tumorigenic in nature.

M1 vs M2 Phenotype Paradigm

Finally, additional testing is needed to explore how M2 macrophages are phenotypically altered following infection by VSV. Our gene expression data revealed differences between M1 and M2 macrophage phenotypes both before and after infection with rwt and rM51R-M viruses. A list of genes was selected to address changes in expression of key polarization transcripts among M1 and M2 macrophages. A simple search of the AmiGO Gene Ontology database for the keyword macrophage reveals 2,485 known genes that are specifically produced by macrophages and 10,221 annotations of additional factors that may influence or be influenced by macrophages. Analysis of larger data sets enable continued exploration of the M1 versus M2 paradigm and the possibility that macrophage populations that survive virus infection may be moving toward some intermediate or alternative phenotype with M1- and M2-like characteristics.

REFERENCES

1. Chavez-Galan L, Olleros ML, Vesin D, Garcia I. 2015. Much More than M1 and M2 Macrophages, There are also CD169(+) and TCR(+) Macrophages. Front Immunol 6:263.
2. Roszer T. 2015. Understanding the Mysterious M2 Macrophage through Activation Markers and Effector Mechanisms. Mediators Inflamm 2015:816460.
3. Ambarus CA, Krausz S, van Eijk M, Hamann J, Radstake TR, Reedquist KA, Tak PP, Baeten DL. 2012. Systematic validation of specific phenotypic markers for in vitro polarized human macrophages. J Immunol Methods 375:196-206.
4. Jablonski KA, Amici SA, Webb LM, Ruiz-Rosado Jde D, Popovich PG, Partida-Sanchez S, Guerau-de-Arellano M. 2015. Novel Markers to Delineate Murine M1 and M2 Macrophages. PLoS One 10:e0145342.
5. Tarique AA, Logan J, Thomas E, Holt PG, Sly PD, Fantino E. 2015. Phenotypic, functional, and plasticity features of classical and alternatively activated human macrophages. Am J Respir Cell Mol Biol 53:676-88.
6. Mantovani A, Biswas SK, Galdiero MR, Sica A, Locati M. 2013. Macrophage plasticity and polarization in tissue repair and remodelling. J Pathol 229:176-85.
7. Bi Y, Chen J, Hu F, Liu J, Li M, Zhao L. 2019. M2 Macrophages as a Potential Target for Antiatherosclerosis Treatment. Neural Plast 2019:6724903.
8. Grimshaw MJ, Balkwill FR. 2001. Inhibition of monocyte and macrophage chemotaxis by hypoxia and inflammation--a potential mechanism. Eur J Immunol 31:480-9.

9. Albini A, Bruno A, Noonan DM, Mortara L. 2018. Contribution to Tumor Angiogenesis From Innate Immune Cells Within the Tumor Microenvironment: Implications for Immunotherapy. Front Immunol 9:527.

10. Wolf GL. 2019. Macrophages hold the key to cancer's inner sanctum. Med Hypotheses 122:111-114.

11. Aras S, Zaidi MR. 2017. TAMeless traitors: macrophages in cancer progression and metastasis. Br J Cancer 117:1583-1591.

12. Kim J, Bae JS. 2016. Tumor-Associated Macrophages and Neutrophils in Tumor Microenvironment. Mediators Inflamm 2016:6058147.

13. Lin Y, Xu J, Lan H. 2019. Tumor-associated macrophages in tumor metastasis: biological roles and clinical therapeutic applications. J Hematol Oncol 12:76.

14. Yang L, Zhang Y. 2017. Tumor-associated macrophages: from basic research to clinical application. J Hematol Oncol 10:58.

15. Murphy DA, Courtneidge SA. 2011. The 'ins' and 'outs' of podosomes and invadopodia: characteristics, formation and function. Nat Rev Mol Cell Biol 12:413-26.

16. Gawden-Bone C, Zhou Z, King E, Prescott A, Watts C, Lucocq J. 2010. Dendritic cell podosomes are protrusive and invade the extracellular matrix using metalloproteinase MMP-14. J Cell Sci 123:1427-37.

17. Thatcher SE, Black JE, Tanaka H, Kohama K, Fultz ME, Cassis LA, Wright GL. 2017. Matrix Metalloproteinases -14, -9 and -2 are Localized to the Podosome and Involved in Podosome Development in the A7r5 Smooth Muscle Cell. J Cardiobiol 5.

18. Wiesner C, Le-Cabec V, El Azzouzi K, Maridonneau-Parini I, Linder S. 2014. Podosomes in space: macrophage migration and matrix degradation in 2D and 3D settings. Cell Adh Migr 8:179-91.

19. Linder S, Kopp P. 2005. Podosomes at a glance. J Cell Sci 118:2079-82.

20. Luxenburg C, Winograd-Katz S, Addadi L, Geiger B. 2012. Involvement of actin polymerization in podosome dynamics. J Cell Sci 125:1666-72.

21. Linder S, Cervero P. 2020. The podosome cap: past, present, perspective. Eur J Cell Biol 99:151087.

22. Alonso F, Spuul P, Daubon T, Kramer I, Genot E. 2019. Variations on the theme of podosomes: A matter of context. Biochim Biophys Acta Mol Cell Res 1866:545-553.

23. Walde M, Monypenny J, Heintzmann R, Jones GE, Cox S. 2014. Vinculin binding angle in podosomes revealed by high resolution microscopy. PLoS One 9:e88251.

24. Van Goethem E, Guiet R, Balor S, Charriere GM, Poincloux R, Labrousse A, Maridonneau-Parini I, Le Cabec V. 2011. Macrophage podosomes go 3D. Eur J Cell Biol 90:224-36.

25. Collin O, Na S, Chowdhury F, Hong M, Shin ME, Wang F, Wang N. 2008. Self-organized podosomes are dynamic mechanosensors. Curr Biol 18:1288-94.

26. Dehring DA, Clarke F, Ricart BG, Huang Y, Gomez TS, Williamson EK, Hammer DA, Billadeau DD, Argon Y, Burkhardt JK. 2011. Hematopoietic lineage cell-specific protein 1 functions in concert with the Wiskott-Aldrich syndrome protein to promote podosome array organization and chemotaxis in dendritic cells. J Immunol 186:4805-18.

27. Hammarfjord O, Falet H, Gurniak C, Hartwig JH, Wallin RP. 2011. Gelsolin-independent podosome formation in dendritic cells. PLoS One 6:e21615.

28. Morton PE, Parsons M. 2011. Dissecting cell adhesion architecture using advanced imaging techniques. Cell Adh Migr 5:351-9.

29. Cougoule C, Van Goethem E, Le Cabec V, Lafouresse F, Dupre L, Mehraj V, Mege JL, Lastrucci C, Maridonneau-Parini I. 2012. Blood leukocytes and macrophages of various phenotypes have distinct abilities to form podosomes and to migrate in 3D environments. Eur J Cell Biol 91:938-49.

30. Linder S, Wiesner C. 2016. Feel the force: Podosomes in mechanosensing. Exp Cell Res 343:67-72.

31. Van Audenhove I, Debeuf N, Boucherie C, Gettemans J. 2015. Fascin actin bundling controls podosome turnover and disassembly while cortactin is involved in podosome assembly by its SH3 domain in THP-1 macrophages and dendritic cells. Biochim Biophys Acta 1853:940-52.

32. Cervero P, Wiesner C, Bouissou A, Poincloux R, Linder S. 2018. Lymphocyte-specific protein 1 regulates mechanosensory oscillation of podosomes and actin isoform-based actomyosin symmetry breaking. Nat Commun 9:515.

33. Bhuwania R, Cornfine S, Fang Z, Kruger M, Luna EJ, Linder S. 2012. Supervillin couples myosin-dependent contractility to podosomes and enables their turnover. J Cell Sci 125:2300-14.

34. Chen X, Liu H, Focia PJ, Shim AH, He X. 2008. Structure of macrophage colony stimulating factor bound to FMS: diverse signaling assemblies of class III receptor tyrosine kinases. Proc Natl Acad Sci U S A 105:18267-72.

35. Chaudhuri A. 2014. Regulation of Macrophage Polarization by RON Receptor Tyrosine Kinase Signaling. Front Immunol 5:546.

36. Brandt DT, Goerke A, Heuer M, Gimona M, Leitges M, Kremmer E, Lammers R, Haller H, Mischak H. 2003. Protein kinase C delta induces Src kinase activity via activation of the protein tyrosine phosphatase PTP alpha. J Biol Chem 278:34073-8.

37. Huang W, Ishii I, Zhang WY, Sonobe M, Kruth HS. 2002. PMA activation of macrophages alters macrophage metabolism of aggregated LDL. J Lipid Res 43:1275-82.

38. Pixley FJ. 2012. Macrophage Migration and Its Regulation by CSF-1. Int J Cell Biol 2012:501962.

39. Cougoule C, Le Cabec V, Poincloux R, Al Saati T, Mege JL, Tabouret G, Lowell CA, Laviolette-Malirat N, Maridonneau-Parini I. 2010. Three-dimensional migration of macrophages requires Hck for podosome organization and extracellular matrix proteolysis. Blood 115:1444-52.

40. Duong LT, Rodan GA. 2000. PYK2 is an adhesion kinase in macrophages, localized in podosomes and activated by beta(2)-integrin ligation. Cell Motil Cytoskeleton 47:174-88.

41. Mitra SK, Hanson DA, Schlaepfer DD. 2005. Focal adhesion kinase: in command and control of cell motility. Nat Rev Mol Cell Biol 6:56-68.

42. Takenawa T, Suetsugu S. 2007. The WASP-WAVE protein network: connecting the membrane to the cytoskeleton. Nat Rev Mol Cell Biol 8:37-48.

43. Abshire MY, Thomas KS, Owen KA, Bouton AH. 2011. Macrophage motility requires distinct alpha5beta1/FAK and alpha4beta1/paxillin signaling events. J Leukoc Biol 89:251-7.

44. Blangy A, Touaitahuata H, Cres G, Pawlak G. 2012. Cofilin activation during podosome belt formation in osteoclasts. PLoS One 7:e45909.

45. Burger KL, Davis AL, Isom S, Mishra N, Seals DF. 2011. The podosome marker protein Tks5 regulates macrophage invasive behavior. Cytoskeleton (Hoboken) 68:694-711.

46. Rafiq NB, Lieu ZZ, Jiang T, Yu CH, Matsudaira P, Jones GE, Bershadsky AD. 2017. Podosome assembly is controlled by the GTPase ARF1 and its nucleotide exchange factor ARNO. J Cell Biol 216:181-197.

47. Sumida GM, Yamada S. 2015. Rho GTPases and the downstream effectors actin-related protein 2/3 (Arp2/3) complex and myosin II induce membrane fusion at self-contacts. J Biol Chem 290:3238-47.

48. Tsuboi S. 2007. Requirement for a complex of Wiskott-Aldrich syndrome protein (WASP) with WASP interacting protein in podosome formation in macrophages. J Immunol 178:2987-95.

49. Vijayakumar V, Monypenny J, Chen XJ, Machesky LM, Lilla S, Thrasher AJ, Anton IM, Calle Y, Jones GE. 2015. Tyrosine phosphorylation of WIP releases bound WASP and impairs podosome assembly in macrophages. J Cell Sci 128:251-65.

50. Poincloux R, Vincent C, Labrousse A, Castandet J, Rigo M, Cougoule C, Bordier C, Le Cabec V, Maridonneau-Parini I. 2006. Re-arrangements of podosome structures are observed when Hck is activated in myeloid cells. Eur J Cell Biol 85:327-32.

51. Pollard TD, Borisy GG. 2003. Cellular motility driven by assembly and disassembly of actin filaments. Cell 112:453-65.

52. Panchal SC, Kaiser DA, Torres E, Pollard TD, Rosen MK. 2003. A conserved amphipathic helix in WASP/Scar proteins is essential for activation of Arp2/3 complex. Nat Struct Biol 10:591-8.

53. Nusblat LM, Dovas A, Cox D. 2011. The non-redundant role of N-WASP in podosome-mediated matrix degradation in macrophages. Eur J Cell Biol 90:205-12.

54. Dovas A, Gevrey JC, Grossi A, Park H, Abou-Kheir W, Cox D. 2009. Regulation of podosome dynamics by WASp phosphorylation: implication in matrix degradation and chemotaxis in macrophages. J Cell Sci 122:3873-82.

55. Linder S, Nelson D, Weiss M, Aepfelbacher M. 1999. Wiskott-Aldrich syndrome protein regulates podosomes in primary human macrophages. Proc Natl Acad Sci U S A 96:9648-53.

56. Clark ES, Whigham AS, Yarbrough WG, Weaver AM. 2007. Cortactin is an essential regulator of matrix metalloproteinase secretion and extracellular matrix degradation in invadopodia. Cancer Res 67:4227-35.

57. Huber LA, Pimplikar S, Parton RG, Virta H, Zerial M, Simons K. 1993. Rab8, a small GTPase involved in vesicular traffic between the TGN and the basolateral plasma membrane. J Cell Biol 123:35-45.

58. Linder S, Hufner K, Wintergerst U, Aepfelbacher M. 2000. Microtubule-dependent formation of podosomal adhesion structures in primary human macrophages. J Cell Sci 113 Pt 23:4165-76.

59. El Azzouzi K, Wiesner C, Linder S. 2016. Metalloproteinase MT1-MMP islets act as memory devices for podosome reemergence. J Cell Biol 213:109-25.

60. Gong Y, Hart E, Shchurin A, Hoover-Plow J. 2008. Inflammatory macrophage migration requires MMP-9 activation by plasminogen in mice. J Clin Invest 118:3012-24.

61. Destaing O, Saltel F, Geminard JC, Jurdic P, Bard F. 2003. Podosomes display actin turnover and dynamic self-organization in osteoclasts expressing actin-green fluorescent protein. Mol Biol Cell 14:407-16.

62. Panzer L, Trube L, Klose M, Joosten B, Slotman J, Cambi A, Linder S. 2016. The formins FHOD1 and INF2 regulate inter- and intra-structural contractility of podosomes. J Cell Sci 129:298-313.

63. Calle Y, Burns S, Thrasher AJ, Jones GE. 2006. The leukocyte podosome. Eur J Cell Biol 85:151-7.

64. Polzin M, McCanless J, Owen S, Sizemore D, Lucero E, Fuller R, Neufeld HS, Seals DF, Ahmed M. 2020. Oncolytic vesicular stomatitis viruses selectively target M2 macrophages. Virus Res doi:10.1016/j.virusres.2020.197991:197991.

65. Lewis JS, Landers RJ, Underwood JC, Harris AL, Lewis CE. 2000. Expression of vascular endothelial growth factor by macrophages is up-regulated in poorly vascularized areas of breast carcinomas. J Pathol 192:150-8.

66. Condeelis J, Pollard JW. 2006. Macrophages: obligate partners for tumor cell migration, invasion, and metastasis. Cell 124:263-6.

67. Binnewies M, Roberts EW, Kersten K, Chan V, Fearon DF, Merad M, Coussens LM, Gabrilovich DI, Ostrand-Rosenberg S, Hedrick CC, Vonderheide RH, Pittet MJ, Jain

RK, Zou WP, Howcroft TK, Woodhouse EC, Weinberg RA, Krummel MF. 2018. Understanding the tumor immune microenvironment (TIME) for effective therapy. Nature Medicine 24:541-550.

68. Meirson T, Gil-Henn H. 2018. Targeting invadopodia for blocking breast cancer metastasis. Drug Resist Updat 39:1-17.

69. Esfahani K, Roudaia L, Buhlaiga N, Del Rincon SV, Papneja N, Miller WH, Jr. 2020. A review of cancer immunotherapy: from the past, to the present, to the future. Curr Oncol 27:S87-S97.

70. Eager RM, Nemunaitis J. 2011. Clinical development directions in oncolytic viral therapy. Cancer Gene Ther 18:305-17.

71. Wojton J, Kaur B. 2010. Impact of tumor microenvironment on oncolytic viral therapy. Cytokine Growth Factor Rev 21:127-34.

72. Diaz RM, Galivo F, Kottke T, Wongthida P, Qiao J, Thompson J, Valdes M, Barber G, Vile RG. 2007. Oncolytic immunovirotherapy for melanoma using vesicular stomatitis virus. Cancer Res 67:2840-8.

73. Lin E, Nemunaitis J. 2004. Oncolytic viral therapies. Cancer Gene Ther 11:643-64.

74. Aghi M, Martuza RL. 2005. Oncolytic viral therapies - the clinical experience. Oncogene 24:7802-16.

75. Parker JN, Bauer DF, Cody JJ, Markert JM. 2009. Oncolytic viral therapy of malignant glioma. Neurotherapeutics 6:558-69.

76. Durham NM, Mulgrew K, McGlinchey K, Monks NR, Ji H, Herbst R, Suzich J, Hammond SA, Kelly EJ. 2017. Oncolytic VSV Primes Differential Responses to Immuno-oncology Therapy. Mol Ther 25:1917-1932.

77. Bell JC, Lichty B, Stojdl D. 2003. Getting oncolytic virus therapies off the ground. Cancer Cell 4:7-11.

78. Moussavi M, Fazli L, Tearle H, Guo Y, Cox M, Bell J, Ong C, Jia W, Rennie PS. 2010. Oncolysis of prostate cancers induced by vesicular stomatitis virus in PTEN knockout mice. Cancer Res 70:1367-76.

79. Randle RW, Northrup SA, Sirintrapun SJ, Lyles DS, Stewart JHt. 2013. Oncolytic vesicular stomatitis virus as a treatment for neuroendocrine tumors. Surgery 154:1323-29; discussion 1329-30.

80. Lech PJ, Russell SJ. 2010. Use of attenuated paramyxoviruses for cancer therapy. Expert Rev Vaccines 9:1275-302.

81. Lichty BD, Power AT, Stojdl DF, Bell JC. 2004. Vesicular stomatitis virus: re-inventing the bullet. Trends Mol Med 10:210-6.

82. Melzer MK, Lopez-Martinez A, Altomonte J. 2017. Oncolytic Vesicular Stomatitis Virus as a Viro-Immunotherapy: Defeating Cancer with a "Hammer" and "Anvil". Biomedicines 5.

83. Finkelshtein D, Werman A, Novick D, Barak S, Rubinstein M. 2013. LDL receptor and its family members serve as the cellular receptors for vesicular stomatitis virus. Proc Natl Acad Sci U S A 110:7306-11.

84. Arnheiter H, Davis NL, Wertz G, Schubert M, Lazzarini RA. 1985. Role of the nucleocapsid protein in regulating vesicular stomatitis virus RNA synthesis. Cell 41:259-67.

85. Green TJ, Rowse M, Tsao J, Kang J, Ge P, Zhou ZH, Luo M. 2011. Access to RNA encapsidated in the nucleocapsid of vesicular stomatitis virus. J Virol 85:2714-22.

86. Kandasamy RK, Vladimer GI, Snijder B, Muller AC, Rebsamen M, Bigenzahn JW, Moskovskich A, Sabler M, Stefanovic A, Scorzoni S, Bruckner M, Penz T, Cleary C, Kralovics R, Colinge J, Bennett KL, Superti-Furga G. 2016. A time-resolved molecular map of the macrophage response to VSV infection. NPJ Syst Biol Appl 2:16027.

87. Black BL, Rhodes RB, McKenzie M, Lyles DS. 1993. The role of vesicular stomatitis virus matrix protein in inhibition of host-directed gene expression is genetically separable from its function in virus assembly. J Virol 67:4814-21.

88. Ahmed M, Lyles DS. 1998. Effect of vesicular stomatitis virus matrix protein on transcription directed by host RNA polymerases I, II, and III. J Virol 72:8413-9.

89. Perry AK, Chen G, Zheng D, Tang H, Cheng G. 2005. The host type I interferon response to viral and bacterial infections. Cell Res 15:407-22.

90. McNab F, Mayer-Barber K, Sher A, Wack A, O'Garra A. 2015. Type I interferons in infectious disease. Nat Rev Immunol 15:87-103.

91. Teijaro JR. 2016. Type I interferons in viral control and immune regulation. Curr Opin Virol 16:31-40.

92. Lund JM, Alexopoulou L, Sato A, Karow M, Adams NC, Gale NW, Iwasaki A, Flavell RA. 2004. Recognition of single-stranded RNA viruses by Toll-like receptor 7. Proc Natl Acad Sci U S A 101:5598-603.

93. Shi Z, Cai Z, Sanchez A, Zhang T, Wen S, Wang J, Yang J, Fu S, Zhang D. 2011. A novel Toll-like receptor that recognizes vesicular stomatitis virus. J Biol Chem 286:4517-24.

94. Olejnik J, Hume AJ, Muhlberger E. 2018. Toll-like receptor 4 in acute viral infection: Too much of a good thing. PLoS Pathog 14:e1007390.

95. Hastie E, Grdzelishvili VZ. 2012. Vesicular stomatitis virus as a flexible platform for oncolytic virotherapy against cancer. J Gen Virol 93:2529-2545.

96. Gray Z, Tabarraei A, Moradi A, Kalani MR. 2019. M51R and Delta-M51 matrix protein of the vesicular stomatitis virus induce apoptosis in colorectal cancer cells. Mol Biol Rep 46:3371-3379.

97. Kopecky SA, Willingham MC, Lyles DS. 2001. Matrix protein and another viral component contribute to induction of apoptosis in cells infected with vesicular stomatitis virus. J Virol 75:12169-81.

98. Stojdl DF, Lichty BD, tenOever BR, Paterson JM, Power AT, Knowles S, Marius R, Reynard J, Poliquin L, Atkins H, Brown EG, Durbin RK, Durbin JE, Hiscott J, Bell JC. 2003. VSV strains with defects in their ability to shutdown innate immunity are potent systemic anti-cancer agents. Cancer Cell 4:263-75.

99. Haller O, Staeheli P, Kochs G. 2007. Interferon-induced Mx proteins in antiviral host defense. Biochimie 89:812-8.

100. Owen S. 2020. The Type I Interferon Anti-Viral Pathway Controbute to Macrophage Polarization Following Infection with Oncolytic Vesicular Stomatitis Virus. Master of Science. Appalachian State University, NC Docks.

101. Whitlow ZW, Connor JH, Lyles DS. 2006. Preferential translation of vesicular stomatitis virus mRNAs is conferred by transcription from the viral genome. J Virol 80:11733-42.

102. Puddington L, Bevan MJ, Rose JK, Lefrancois L. 1986. N protein is the predominant antigen recognized by vesicular stomatitis virus-specific cytotoxic T cells. J Virol 60:708-17.

103. Ochoa GC, Slepnev VI, Neff L, Ringstad N, Takei K, Daniell L, Kim W, Cao H, McNiven M, Baron R, De Camilli P. 2000. A functional link between dynamin and the actin cytoskeleton at podosomes. J Cell Biol 150:377-89.

104. Webb BA, Eves R, Mak AS. 2006. Cortactin regulates podosome formation: roles of the protein interaction domains. Exp Cell Res 312:760-9.

105. Zalli D, Neff L, Nagano K, Shin NY, Witke W, Gori F, Baron R. 2016. The Actin-Binding Protein Cofilin and Its Interaction With Cortactin Are Required for Podosome Patterning in Osteoclasts and Bone Resorption In Vivo and In Vitro. J Bone Miner Res 31:1701-12.

106. Tristan C, Shahani N, Sedlak TW, Sawa A. 2011. The diverse functions of GAPDH: views from different subcellular compartments. Cell Signal 23:317-23.

107. Chanput W, Mes JJ, Wichers HJ. 2014. THP-1 cell line: an in vitro cell model for immune modulation approach. Int Immunopharmacol 23:37-45.

108. Lin J, Liu J, Wang Y, Zhu J, Zhou K, Smith N, Zhan X. 2005. Differential regulation of cortactin and N-WASP-mediated actin polymerization by missing in metastasis (MIM) protein. Oncogene 24:2059-66.

109. Taylor MJ, Lampe M, Merrifield CJ. 2012. A feedback loop between dynamin and actin recruitment during clathrin-mediated endocytosis. PLoS Biol 10:e1001302.

110. Montezano AC, Touyz RM. 2013. Mechanosensitive regulation of cortactin by p47phox: a new paradigm in cytoskeletal remodeling. Circ Res 112:1522-5.

111. Kelly D, Pollard AJ. 2003. W135 in Africa: origins, problems and perspectives. Travel Med Infect Dis 1:19-28.

112. Wu X, Suetsugu S, Cooper LA, Takenawa T, Guan JL. 2004. Focal adhesion kinase regulation of N-WASP subcellular localization and function. J Biol Chem 279:9565-76.

113. Verollet C, Charriere GM, Labrousse A, Cougoule C, Le Cabec V, Maridonneau-Parini I. 2011. Extracellular proteolysis in macrophage migration: losing grip for a breakthrough. Eur J Immunol 41:2805-13.

114. Gaffney J, Solomonov I, Zehorai E, Sagi I. 2015. Multilevel regulation of matrix metalloproteinases in tissue homeostasis indicates their molecular specificity in vivo. Matrix Biol 44-46:191-9.

115. Pelaez R, Pariente A, Perez-Sala A, Larrayoz IM. 2019. Integrins: Moonlighting Proteins in Invadosome Formation. Cancers (Basel) 11.

116. Wissing TB, Bonito V, van Haaften EE, van Doeselaar M, Brugmans M, Janssen HM, Bouten CVC, Smits A. 2019. Macrophage-Driven Biomaterial Degradation Depends on Scaffold Microarchitecture. Front Bioeng Biotechnol 7:87.

117. Cui K, Ardell CL, Podolnikova NP, Yakubenko VP. 2018. Distinct Migratory Properties of M1, M2, and Resident Macrophages Are Regulated by alphaDbeta2 and alphaMbeta2 Integrin-Mediated Adhesion. Front Immunol 9:2650.

118. Bear JE, Haugh JM. 2014. Directed migration of mesenchymal cells: where signaling and the cytoskeleton meet. Curr Opin Cell Biol 30:74-82.

119. Ma Z, Qin H, Benveniste EN. 2001. Transcriptional suppression of matrix metalloproteinase-9 gene expression by IFN-gamma and IFN-beta: critical role of STAT-1alpha. J Immunol 167:5150-9.

120. Polzin M, McCanless J, Owen S, Sizemore D, Lucero E, Fuller R, Neufeld HS, Seals DF, Ahmed M. 2020. Oncolytic vesicular stomatitis viruses selectively target M2 macrophages. Virus Res 284:197991.

121. Linder S. 2007. The matrix corroded: podosomes and invadopodia in extracellular matrix degradation. Trends Cell Biol 17:107-17.

122. Tsuchiya S, Yamabe M, Yamaguchi Y, Kobayashi Y, Konno T, Tada K. 1980. Establishment and characterization of a human acute monocytic leukemia cell line (THP-1). Int J Cancer 26:171-6.

123. Boyum A. 1968. Isolation of mononuclear cells and granulocytes from human blood. Isolation of monuclear cells by one centrifugation, and of granulocytes by combining centrifugation and sedimentation at 1 g. Scand J Clin Lab Invest Suppl 97:77-89.

124. Marteau JB, Mohr S, Pfister M, Visvikis-Siest S. 2005. Collection and storage of human blood cells for mRNA expression profiling: a 15-month stability study. Clin Chem 51:1250-2.

125. Brandslund I, Rasmussen JM, Fisker D, Svehag SE. 1982. Separation of human peripheral blood monocytes on continuous density gradients of polyvinylpyrrolidone-coated silica gel (Percoll). J Immunol Methods 48:199-211.

126. Hastie E, Grdzelishvili VZ. 2012. Vesicular stomatitis virus as a flexible platform for oncolytic virotherapy against cancer. J Gen Virol 93:2529-45.

127. Huneycutt BS, Bi Z, Aoki CJ, Reiss CS. 1993. Central neuropathogenesis of vesicular stomatitis virus infection of immunodeficient mice. J Virol 67:6698-706.

128. Flanagan EB, Schoeb TR, Wertz GW. 2003. Vesicular stomatitis viruses with rearranged genomes have altered invasiveness and neuropathogenesis in mice. J Virol 77:5740-8.

129. Chauhan VS, Furr SR, Sterka DG, Jr., Nelson DA, Moerdyk-Schauwecker M, Marriott I, Grdzelishvili VZ. 2010. Vesicular stomatitis virus infects resident cells of the central nervous system and induces replication-dependent inflammatory responses. Virology 400:187-96.

130. Johnson JE, Nasar F, Coleman JW, Price RE, Javadian A, Draper K, Lee M, Reilly PA, Clarke DK, Hendry RM, Udem SA. 2007. Neurovirulence properties of recombinant vesicular stomatitis virus vectors in non-human primates. Virology 360:36-49.

131. Leveille S, Goulet ML, Lichty BD, Hiscott J. 2011. Vesicular stomatitis virus oncolytic treatment interferes with tumor-associated dendritic cell functions and abrogates tumor antigen presentation. J Virol 85:12160-9.

132. Boudreau JE, Bridle BW, Stephenson KB, Jenkins KM, Brunelliere J, Bramson JL, Lichty BD, Wan Y. 2009. Recombinant vesicular stomatitis virus transduction of dendritic cells enhances their ability to prime innate and adaptive antitumor immunity. Mol Ther 17:1465-72.

133. Wongthida P, Diaz RM, Pulido C, Rommelfanger D, Galivo F, Kaluza K, Kottke T, Thompson J, Melcher A, Vile R. 2011. Activating systemic T-cell immunity against

self tumor antigens to support oncolytic virotherapy with vesicular stomatitis virus. Hum Gene Ther 22:1343-53.

Vita

Dalton Patrick Sizemore was born in Greensboro, NC, and is the son of Crystal Sizemore and the grandson of Charlie and Mary Lou Sizemore. He graduated from Eastern Guilford High School in 2012. He then proceeded to the University of Mississippi with the goal of achieving a political science degree before transferring to Guilford Technical Community College to obtain transfer credits and then to Appalachian State University where he graduated with his Bachelor of Science in Cell and Molecular Biology in December 2018. In January 2019, Mr. Sizemore commenced work toward his M.S. in Cell and Molecular Biology at Appalachian State University.

While at working toward his M.S. at Appalachian State, Mr. Sizemore served as president of the Biology Graduate Student Association, vice-president and president of the Appalachian State Graduate Student Government Association, chair of the Library Services Committee, and on various committees and panels across the University and State of North Carolina as a voice for graduate students.

Mr. Sizemore has co-founded Verenovo Energy, headquartered in North Wilkesboro, NC, and intends to move there along with his adorable Labrador Retriever, Molly B (short for Molecular Biology).